SRC-2007-04
25 June 2007
Contract/Order No: B2532534
Void Detection Demonstration Projects

Final Report

Look-Ahead-Radar Field Test Report

Prepared for

Christopher Kelly
MSHA Technical Support
Mine Waste and Geotechnical Engineering Division
P.O. Box 18233
626 Cochrans Mill Road
Pittsburgh, Pennsylvania 15236
Kelly.Christopher@dol.gov

Prepared by

Research Corporation

Stolar Research Corporation
848 Clayton Highway
Raton, New Mexico 87740
(505) 445-3607
fax: (505) 445-2038
stolar@stolarhorizon.com

EXECUTIVE SUMMARY

Breakthroughs in the existing state of the art in the detection of abandoned mines have been successfully demonstrated in this U.S. Mine Safety and Health Administration (MSHA) project. The technical problem addressed by this breakthrough is that when an electromagnetic (EM) wave traveling at the speed of light (c) intersects natural media, such as the earth's surface or the recently cut coal face, the EM wave is slowed down and part of the wave is reflected. The part of the EM wave traveling in the slower velocity (υ) medium experiences energy loss (attenuation), intersects the second interface of the abandoned mine and returns to the detecting receiver. Often the reflected EM wave from the first interface is a factor of 1,000 (60 dB) to 10,000 (80 dB) greater than the EM wave reflected from the second interface. The first interface reflected EM wave dominates the weaker reflected wave from the second abandoned mine interface, making the second reflected wave difficult to detect.

The breakthrough is the suppression of the first interface reflected EM wave at the receiver by a factor of 1,000 (60 dB) to 10,000 (80 dB) and the reception of the weaker EM wave reflected from the abandoned mine. The antenna suppression adds to the software-definable transceiver (SDT) radar predistorted waveform and real-time signal processing algorithm that enables at least 60 dB of first interface reflection suppression. Stolar Research Corporation (Stolar) has pioneered these innovations and has demonstrated a Look-Ahead-Radar (LAR) system designed around these breakthroughs in radar design.

The LAR development and demonstration sites were located at the Deer Creek and Sufco Coal Mines near Price, Utah, Consol Energy's No. 84 Mine near Washington, Pennsylvania, and the Bowie Resources Upper B-Seam Mine, near Paonia, Colorado. The results of field tests at these locations indicated that the technical challenges were the physical size of the radar antennas and the requirement to suppress the first air-coal interface reflected wave so that the weaker second interface reflected wave could be detected.

The preliminary demonstration of the RMPA in the Sufco Coal Mine revealed that the attenuation rate was near 1 dB/ft in the coal seam, indicating to the design team that the LAR operating band frequencies needed to be in the 100- to 250-MHz range if the 20-ft void detection range was to be achieved. In this frequency range, the resonant microstrip patch antenna (RMPA) requires a patch length of 30 in. (0.75 m) for a substrate relative dielectric (ε_r) constant of 4. The length decreases to 20 in. (0.5 m) for an ε_r of 9. These dimensions were far too large for a cutting drum-mounted LAR. This finding caused a search for antenna structures with dimensions close to 6 in. (0.15 m). The following microwave antennas were theoretically investigated, designed, built, and tested:

- Dielectrically loaded horn antennas
- Dual-sleeve dipoles
- Folded RMPA antennas
- Spiral antennas.

The sleeve dipole exhibited a back lobe and machine body loading that was unacceptable for drum mounting. When made small enough for the application, the dielectrically loaded horn exhibited poor EM radiation efficiency. The folded RMPA exhibited poor efficiency. After a review of the laboratory and in-mine demonstration data, a spiral antenna design was recommended and entered into a development program. The technical challenge was the requisition of extremely low-loss dielectric materials for the spiral antenna substrate. The lead time for acquiring a substrate with an effective dielectric permittivity of 12 was estimated by the manufacturer to be in excess of 3 to 4 months. This lead time was past the scheduled demonstration date, requiring that Stolar build longer spiral antennas with a relative dielectric permittivity of 4.

The SDT radar was developed to enable confirmation of the first interface reflection suppression and detection of the second interface reflection. These capabilities were demonstrated at the No. 84 Mine with some effectiveness. However, time did not permit the full optimization of the SDT radar electronics, and Stolar considers the field test conclusions sub-optimal. After this demonstration, the system was optimized for electrical performance, antenna matching, radar algorithm processing, and graphical user interface performance. Laboratory tests proved that 100 dB of suppression could be achieved with the SDT LAR. This improved system was demonstrated at the Bowie Mine in late February. The results of that final field demonstration of the prototype LAR system are described in this report.

The LAR test plan was approved by the regional MSHA office for two in-mine sites. The first site was a pie-shaped block of coal enabling radar operating range tests up to 33 ft (10 m). The approved mining plan required the wire mesh to be installed on the rib. During the final in-mine test, plastic containers filled with water were stacked along this rib. These containers were used in an attempt to simulate a water-filled void opposite an active coal mining face. The second test site was designed to monitor the continuous mining machine while it developed a crosscut during actual mining. The LAR was set up to detect the closing distance of the second interface—the air-coal boundary.

The most important graphic in this entire report, Figure ES-1, shows the reflection conditions as the CM is trammed as far back from the mining face as possible. The mining face known to exist at a distance of 30 ft (9 m) from the LAR is an obvious reflection plane in the display and the position of the CM is confirmed by the secondary reflection at the 38-ft marker. The peak at 50 ft is the coal buggy.

Although a “hand-held” version of the radar was the initial objective of the program, the ultimate size of the antennas left the LAR system as merely “portable,” With an antenna redesign Stolar feels that both hand-held and machine-mounted versions are within reach.

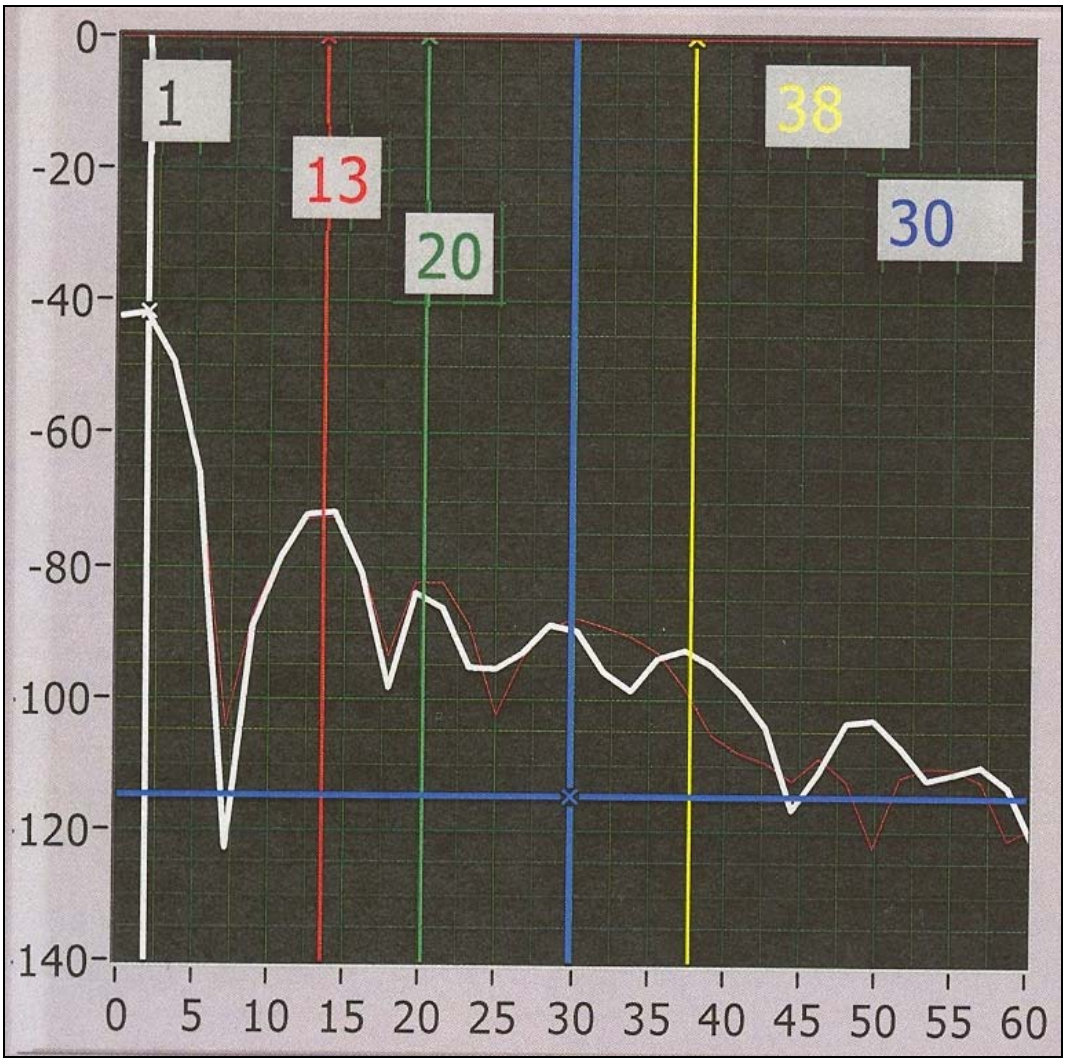

Figure ES-1. LAR display of a true air-coal reflection at the 30-ft distance marker. The mining face was established at this position and the CM was backed away (38-ft reflection). The face reflection (blue cursor) results entirely from the mining face.

This graphic is positive proof that the air-coal interface of the freshly cut mining face is detectable by the prototype LAR system, even with the false positives created by the stationary peaks of its local reflectors in the near-field. The air-coal interface is not augmented by water, roof bolts, or mining equipment; also it is a fairly narrow reflector (crosscut width) compared to the reflecting interface that would be created by an entire entry, as seen in side view. In addition, this 30-ft (9 m) detection distance is 10 ft (1 m) beyond the initial objective of the program (20-ft standard). This is not to imply that 30 ft (9 m) is the maximum capability of LAR in this coal seam, but rather the distance immediately supported by the logistics of this testing scenario and the limitations of the procedure during the dynamic site demonstration.

CONTENTS

APPENDICES

LIST OF FIGURES

LIST OF TABLES

LIST OF TERMS

A	Power amperage
BT	Bluetooth wireless serial link
CM	Continuous miner
DDS	direct digital synthesizer
EM	electromagnetic
FMCW	frequency modulated, continuous wave
FPGA	field-programmable gate array
GPR	ground-penetrating radar
HS-LAR	Horizon-Sensor-Look-Ahead Radar
IAP	in-application programming
IS	intrinsically safe
LAR	Look-Ahead-Radar
LHCP	left-hand circular polarized
LUT	look-up table
MSHA	U. S. Mine Safety and Health Administration
NEC	Numerical Electromagnetics Code
PA	power amplifier
PC	Laptop personal computer
PCB	printed circuit board
PDA	Personal digital assistant
RHCP	right-hand circular polarized
RMPA	resonant microstrip patch antenna
RX	LAR receiving antenna
SA	Spectrum analyzer
SDT	software-definable transceiver
SG	Signal generator
SFCW	Stepped-frequency continuous wave
Stolar	Stolar Research Corporation
TX	LAR transmitting antenna
VAC	AC power voltage
VDC	DC power voltage
XC	cross-cut
XHCP	(left-hand or right-hand) circular polarized

1.0 INTRODUCTION

The energy-production challenges facing the coal mining and methane-extraction industries are highlighted in Senator Pete V. Domenici's book, *A Brighter Tomorrow* (1). As chairman of the Senate Energy Committee, Senator Domenici receives an endless parade of highly qualified executives, scientists, and engineers who inform him about energy supply and demand for decades in the future. Of the books that have been written on the subject, his is about the best at predicting the future needs for coal and hydrocarbons. U.S. energy demands for coal and coal-bed methane are increasing faster than 1.8 percent per year. To meet this demand for energy, production will need to be increased by more than 46 percent by the year 2025.

Although energy experts believe that coal is abundant, the truth is quite different. The rate at which the U.S. is depleting its coal reserves has been underestimated. In the Raton Coal Basin, the cavitation method of coal-bed methane production has spoiled more than 1 billion mineable tons of coal—about 1 year's U.S. coal production. Extracting 5 percent of the coal bed methane (CBM) British thermal units (BTU) using high-pressure cavitation spoils 95 percent of the coal BTUs. Elsewhere, the easy-to-mine coal reserves are nearing exhaustion. Future mining will be in thinner, deeper, more geologically complex coal seams and in areas near abandoned mines. For the coal mining industry to keep up with energy demands, a quantum leap forward in mining technology will be needed.

The technical challenges facing future coal miners are significant and well known to mining personnel who have dedicated lifetimes to solving difficult production and safety problems. The National Mining Association (NMA) executives, in a technology road-mapping session sponsored by the U.S. Department of Energy's (DOE) Mine of the Future program, prioritized technology needed by the industry in future years. The top 10 needed technologies included the following:

- Coal-cutting-edge sensing for selective mining to minimize out-of-seam dilution and improve run-of-mine coal quality. The Quecreek event added the safety need to prevent mining into abandoned coal mines.
- Imaging geologic structures ahead of mining
- Improving directional drilling technology with integrating geophysics instrumentation.

The technical challenge facing the extraction of hydrocarbons using directional drilling is presented in Anderson's *Scientific American* article, "Oil Production in the 21st Century" (2). This section discusses the problem of detecting boundaries in layered coal deposits and detecting abandoned mine voids.

How to detect coal seam boundary sedimentary rock and water-/gas-filled voids has been the focus of research and development programs for more than 46 years (3). The Quecreek coal mining incident awakened the national conscience to the safety requirement of detecting abandoned mine entries ahead of mining (4). The problem is severe; every other week someone

cuts into an abandoned mine. Solving the problem presents significant technical challenges that require breakthroughs in the present state of the art. First and foremost, coal seam beds are undulating geologic structures with complex gradational boundaries. Each ton of coal has 1 billion (^{2} of surface area in its matrix and 100 to 1,000 ft^3 of methane.

The depositional environment of a coal seam includes microbial processes that feature aerobic and anaerobic bacteria accumulation. The processes cause a reducing environment and subsequent sedimentation of heavy metals. Near the coal seam boundary, septic conditions cause thin bounding layers to be contaminated with mercury, sulfur, and ash, as described in Figure 1-1. Leaving this contaminated layer behind improves coal quality and reduces the potential for a roof fall. The contamination also decreases the gas flow permeability near the coal seam boundary.

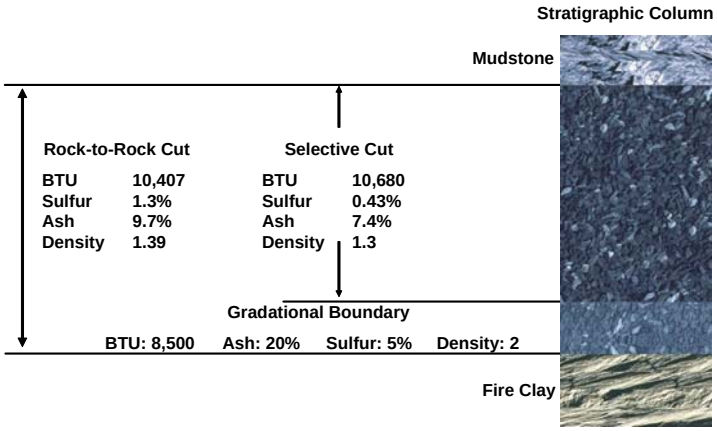

Figure 1-1. Vertical cross section of a coal seam.

Boundary detection requires that sensors be located near the cutting edges of buckets, blades, and rotating drums. Real-time detection of mine voids at least 20 ft (6.1 m) ahead of the coal cutting machine is the design goal of a look-ahead radar (LAR). Because mining at a depth of 40 ft (12 m) is common practice with remote-control continuous mining machines (CM), ground-control safety requires roof bolting before mine personnel can advance into a newly developed entry. From the safety perspective of detecting abandoned mines, the LAR must be integrated into the cutting drum of a CM. If the detection sensors are located far away from the cutting edges, feedback control systems on automated machines and gimbals fail to provide closed-loop control. Full machine automation becomes impracticable.

For void detection ahead of mining, the U.S. Mine Safety and Health Administration (MSHA) requires horizontal directional drilling in mines operating near abandoned mining complexes. In-mine drilling slows down mining processes because it requires relocating and repositioning a drilling machine. The efficiency of longhole horizontal directional drilling to probe for abandoned mine boundaries increases if the borehole can be maintained within the coal bed. An obvious technical solution is to adapt radar to find the abandoned mining complexes and operate the radar near the recently cut face. In-mine demonstrations of portable commercially available ground-penetrating radar (GPR) have conclusively demonstrated that abandoned mines can be detected (5).

Radars designed for installation near the drum's cutting edge are not even a close cousin to GPR. Radar operated for this purpose requires intrinsically safe (IS) or flameproof certification from the MSHA Certification and Approval Center in Tridelphia, West Virginia. Developing a product that achieves this certification requires a highly qualified design team understanding the technical requirements. The intrinsic safety design requirements are not taught in design engineering curricula. As an example of the time required to certify a complex electronic circuit, the engineering team must work with MSHA in an iterative design process that can require more than a year to complete. The IS battery protections approval cycle requires 36 months to complete. The radar must be designed to withstand an exceedingly high g force of vibration and shock, while processing data in real time using fast, autonomous algorithms. Because the radar must be "trialed" under realistic mining and drilling conditions, the electronics design must accommodate software reprogramming while the machine is cutting coal or drilling in hydrocarbon reservoirs. This feature is called remote wireless programming while mining or drilling. The software design industry refers to this advanced concept as in-application programming (IAP). The radar must control the mining machine or gimbal in real time.

Safe and efficient coal extraction requires advanced radar subsystems that can be mounted on cutting drums of coal mining machines. However, applying real-time radar to mining applications has been difficult if not impossible throughout the history of this industry. The critical need to provide miners with an "early-warning" system when in close proximity to abandoned mine voids has become increasingly evident. A specialized radar system that is sensitive to air-filled or water-filled voids ahead of mining would prove a valuable tool and significant safety cushion in the coal mining industry specifically.

Stolar's recent work in this field under the auspices of MSHA's void detection program has led to the field demonstration of a look-ahead radar (LAR) system that must transmit an electromagnetic (EM) wave 20 ft (6.1 m) to detect in-seam voids. The reflected EM wave must be processed in real time to determine the physical distance to the reflector. The radar wave-front must also be blind to the high-level return of the initial air-coal reflection, while remaining sensitive to the low-level reflection from the air-coal or air-water reflection plane on the opposite side of the uncut coal.

The early experimental results in the industry suggested that voids ahead of mining could be detected using a VHF band predistorted EM-wave radar. However, the current LAR system requires confirmation of performance capability and limitations at an active mine site. Stolar has identified an underground test site within the current B-Seam mining operations at Bowie Resources Mine near Paonia, Colorado. Stolar has worked with Bowie to develop a strategic test and demonstration program of the portable LAR's functionality at their mine. These tests occurred in two different sections of the Bowie Mine and consisted of measuring radar reflections of air voids through a tapered pillar block for thickness prediction, and the real-time radar monitoring of a cross-cut break-though for CM-related mining processes. The test instrumentation was used in a fresh-air environment for the first test, and was used inby the last open cross-cut for the second test. "Inby" is a mining term relating to a direction into the mine that is moving away from the surface and further toward the direction of active mining. For example, to work "inby the last open crosscut" suggests that work is occurring past the last open avenue for ventilated fresh air. This suggests that the working atmosphere could be poorly

ventilated and higher in methane than in other areas of the mine outby (moving out of the mine). This scenario is critical since noncertified electrical equipment must not be used in non-fresh-air situations without the proper safeguards and experimental approvals.

2.0 LAR SYSTEM DESCRIPTION

The LAR system uses a compact stepped-frequency, continuous-wave (SFCW) radar design for forward-looking capability with an anticipated minimum range of 20 ft (6.1 m) (dependent on the relative dielectric permittivity of the coal). The SFCW system is a modified frequency-modulated radar design unique to Stolar and incorporates a novel technique to suppress the initial reflected wave from near-field boundaries (the first few feet) and determine the range to a reflecting target using Stolar's new software-definable transceiver (SDT). The operational frequency band of the LAR antennas is between 150 and 250 MHz. The SDT, which is capable of significantly wider operating frequencies, is currently controlled via a laptop personal computer (PC). However, the PC software is reconfigurable for use in a hand-held personal digital assistant (PDA). The SDT radar electronics are shown in Figure 2-1.

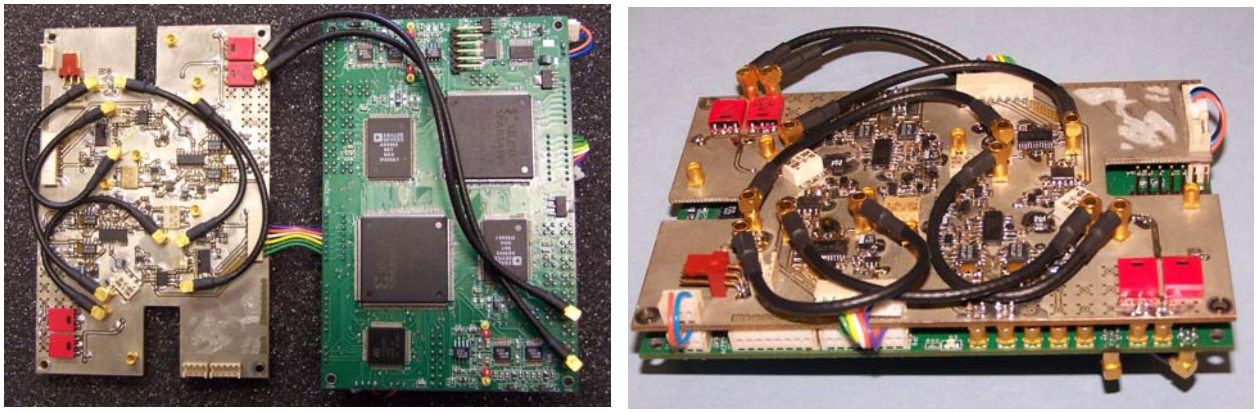

Figure 2-1. SDT radar electronics.

The technical challenge caused by the first interface reflected EM wave needed to be addressed in the LAR system design. The seminal concept presented in this advanced radar design is the transmission of a predistorted radar waveform combined with a software algorithm developed to suppress the reflection from the stress-fracture coal (first interface). As will be mathematically described later, the process involved the precise control of frequency and phase in the pair of continuous waves in the transmit waveform. Control of the magnitude of the pair of continuous waves is required in the predistorted waveform. The results of solving the first interface reflection challenge are illustrated in Figure 2-2 for constant-frequency-difference stepped radar. Curve A is typical processed frequency domain data that has been transformed to the time domain where wave velocity (υ) and round-trip travel time (τ) have determined distance for a conventional SFCW radar reflection from an abandoned mine void located at 17 feet. Curve B is the time domain response results from a predistorted frequency-modulated, continuous-wave (FMCW) or SFCW radar processed to suppress the first interface reflection and reveal the second weaker reflection from the abandoned mine.

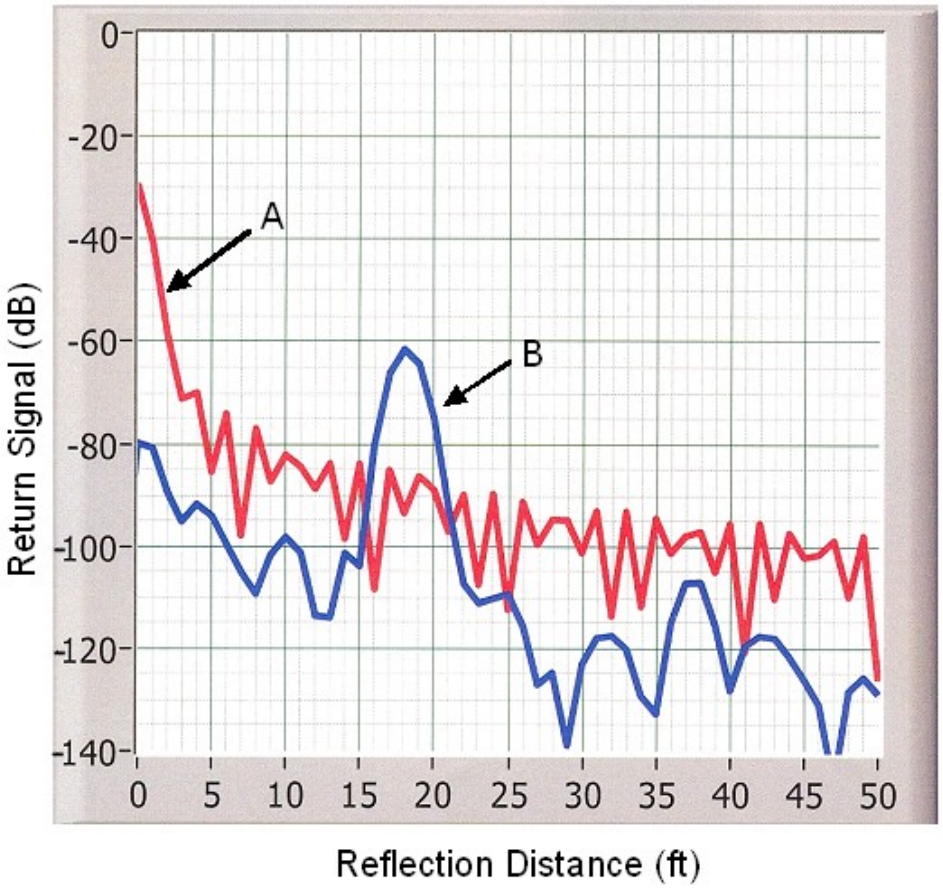

Figure 2-2. SFCW radar requires data transformed from frequency to time domain. Curve A is the near-measurement data and Curve B is the far-measurement data.

In Figure 2-2 the horizontal axis represents the predicted distance from the LAR receiver antenna to the signal reflector. This predicted distance is the quotient of the radar-estimated reflection distance and the square root of the assumed dielectric constant (or relative dielectric permittivity). The vertical axis represents a logarithmic scale for return signal power. A 0-dB level is calibrated to equal the power of the transmitter (before antenna radiation). The -30-dB level is the y-intercept of the return signal (distance equals zero). This is essentially the radiated power of the transmitter antenna. The 30-dB drop in signal level from the input to the output of the transmitter antenna represents the antenna's inefficiency. The -30-dB level can be considered the coupling factor of the radiation, i.e., that power actually entering the coal seam at the initial air-coal boundary. However, the initial reflection from the near-antenna environment will be at a magnitude only slightly lower than the -30dB coupling power (zero-distance in Curve A). This response masks the second interface reflected wave. Essentially the radar has been blinded by the reflection from the first interface for a distance of at least 2.5 ft (0.76 m). Although the first interface reflection predominates the zero-distance response, the near measurement data are useful in determining the electrical conductivity or relative dielectric

permittivity (depends on the loss tangent) of the first coal layer. These data also are used in predistorting the transmitted waveform.

This illustrates that the advanced radar solved two different problems. The predistorted SFCW-response (Figure 2-2, Curve B) indicates that the near-field effect has been suppressed, while the weak reflection from the second interface has been emphasized. The advanced radar has been designed to achieve an in situ measurement of the electrical parameters (conductivity and relative dielectric permittivity) of the natural media next to the antenna and the Curve B response illustrates suppression to enable detection of the second interface reflection.

The Fourier transform or the algorithm that transforms data from the frequency to the time domain is embedded in the radar electronics field-programmable gate array (FPGA). The frequency domain reflected wave is processed in the FPGA, creating the time-domain representation in Figure 2-2, Curve B. The radar electronics features a microprocessor that downloads the program software defining the digital electronic functions of the radar architecture.

The wider the frequency band of the radar, the better the resolution. The range resolution is given by Res where $\mathrm{Re}\,s = \dfrac{1.38c}{2BW\sqrt{\varepsilon_r}}$ where BW is the bandwidth of the instrument and ε_r is the relative dielectric permittivity. The magnitude, frequency, and phase of each frequency component (sinusoidal waveform) are set by the microprocessor to generate the predistorted waveform. The SDT radar can be programmed to generate phase, frequency, or amplitude-modulated predistorted waveforms. The Horizon-Sensor-Look-Ahead Radar (HS-LAR) design generates an amplitude-modulated suppressed carrier waveform, shown in Figure 2-3.

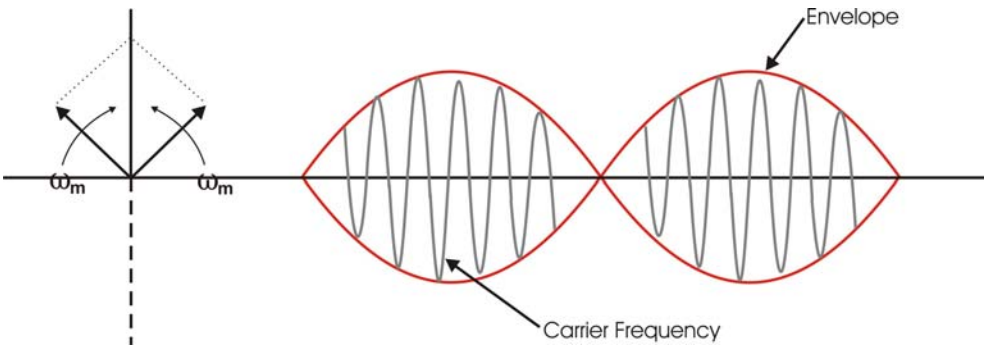

Figure 2-3. Double sideband suppressed carrier waveform.

A prototype implementation of the present system uses a highly integrated digital PCB and a plug-compatible analog PCB. The digital PCB achieves the design requirement of IAP so that software changes and data acquisition can be achieved while mining or drilling. The FPGAs are built into the digital PCB. The digital PCB has two Xilinx[1] FPGAs, an 8-bit host microcontroller with 256 KB of on-chip flash memory, and 12-bit analog-to-digital (A/D) and digital-to-analog

[1]Xilinx is a trademark of Xilinx, Inc., San Jose, California.

(D/A) converters. The design also includes an RS-232 serial communications link and Bluetooth[2] modem. The FPGA logic device replaces tens of standard logic devices and allows functional changes to the peripheral hardware without making any changes to the hardware itself. The combination of these devices allows optimum software and hardware task distribution. In such a configuration, the microcontroller acts as a host processor, governing the FPGA as a reconfigurable universal interface between the board and external devices. Processing software is downloaded onto the digital PCB from LabView.[3] At startup, the microcontroller downloads to the FPGA. Changes to the microcontroller software or FPGA configuration require only the microcontroller to be reprogrammed. The in-system programmable on-chip flash memory of the microcontroller could be reprogrammed through its JTAG interface or through its serial communications link. In-application programming capability could be used to reprogram the PCB remotely through the wireless Bluetooth communications link. The IAP represents an advantage because the radar functionality can be remotely changed quickly and easily.

The FPGA's direct digital synthesizer (DDS) or external DDS achieves the predistortion function if an Analog Devices AD9959 is used. Predistortion generally requires the insertion of a compensating frequency response module before the transmitter RF power amplifier (PA). The predistorter has the inverse response of the PA and antenna, so the overall response is linear. Adaptive digital predistortion involves a digital implementation of the predistorter and a feedback loop for adapting to the changes in the response of the PA and antennas.

The two main types of adaptation algorithms are the "blind adaptive" algorithms based on distance-gradient methods and the "polynomial function" algorithms that attempt to directly model the nonlinearities in the radar forward and reverse transmission paths. The correction factors can be computed using an adaptation algorithm and can be stored in a look-up table (LUT). The LUTs typically are updated dynamically to reduce errors between the predistorter input and the TX antenna output.

The blind adaptive LUT-based approach uses incoming samples (I and Q) with correction factors applied from an LUT and sent to the FPGA or an RF module. The LUT's address is derived from the input power and the LUT contains two values for each location, the real part, I, and the imaginary part, Q. In the feedback loop, samples of the radiated TX signal are used to update the current vales stored in the LUT.

The analog PCB includes a quadrature up-converter, RF power amplifier, coupler (for a monostatic radar), phase locked loop (PLL), or several quad DDSs (Analog Device AD9959) and a down-converter. A simplified block diagram of the SDT radar, including digital and analog printed circuit boards, is shown in Figure 2-4.

[2]Bluetooth is a trademark of Bluetooth Sig., Inc., Belleview, Washington.

[3] LabView is a trademark of National Instruments Corporation, Austin, Texas.

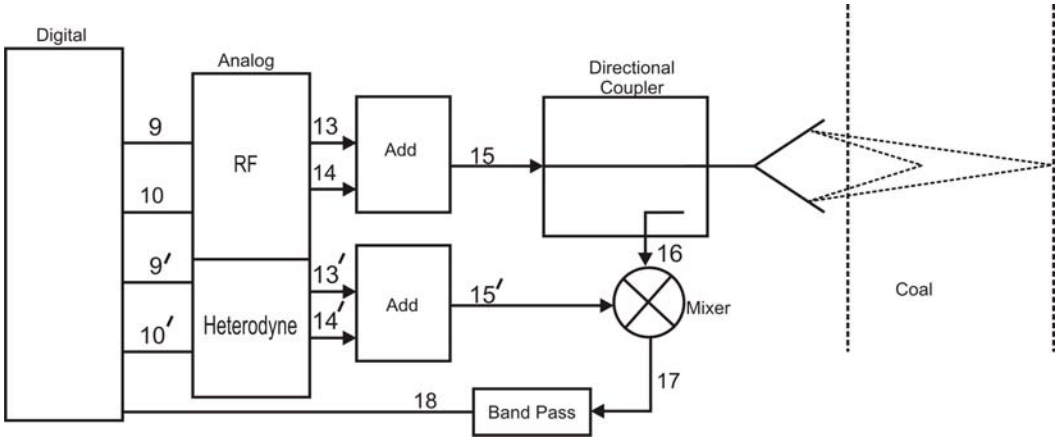

Figure 2-4. Block diagram of SDT radar configuration.

The newest radar antennas are optimized to operate in the required system frequency range. The dielectric material and dual antenna geometry have been optimized and fixed for frequency range and physical size requirements. They also exhibit a better frequency response because of the development of a matching network. The matching network optimizes the power transfer from the electronics to the antenna. Software simulations and mathematical calculations have verified the performance of these new antennas. The matching network is shown in Figure 2-5.

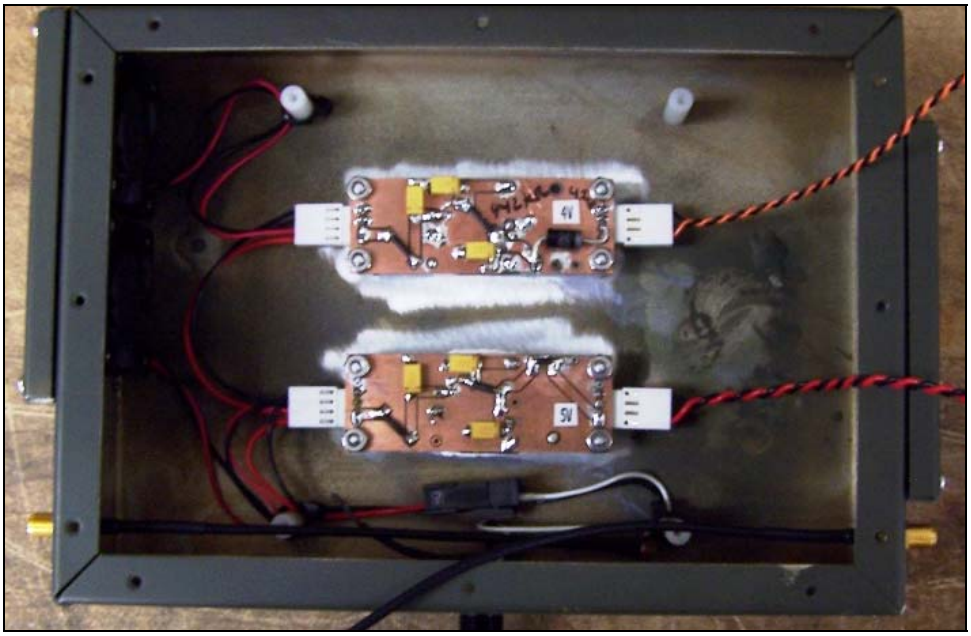

Figure 2-5. LAR matching network for antenna input/output.

The electronics also have been optimized for operation in the system frequency range of the antennas. The electronics have improved sensitivity, increased dynamic range, and reduced power consumption. The PCB design did require several upgrades to maintain RF signal

integrity throughout the layout. The new PCBs are shown in the electronics housing in Figure 2-6.

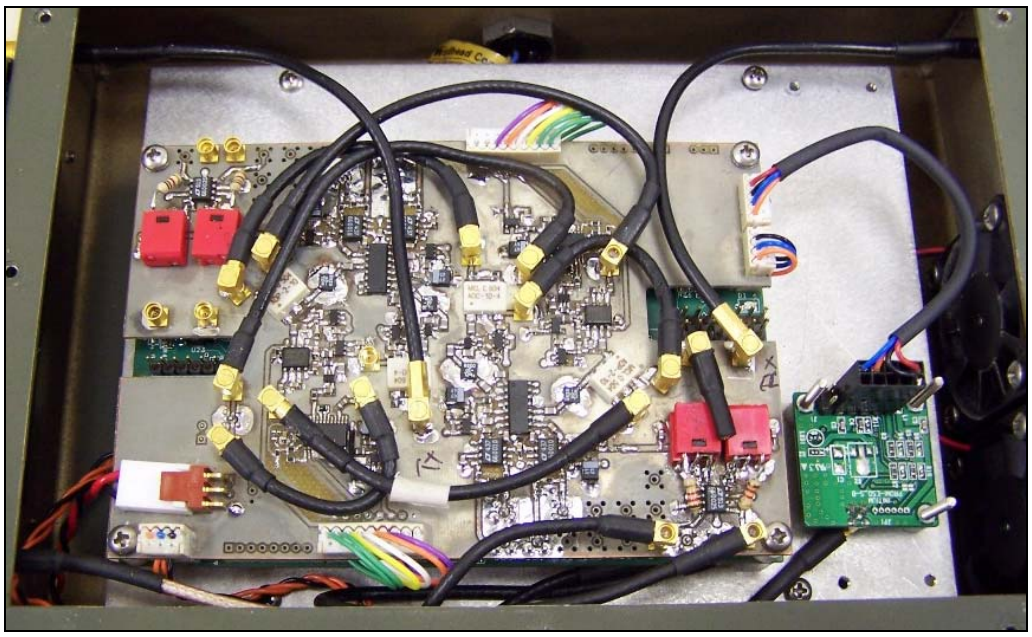

Figure 2-6. SDT radar frequency circuit boards.

The real-time data processing and control software were updated along with the new electronics. Enhancements also were made to the advanced signal processing algorithm. This algorithm was enhanced to correct for the delays encountered in the antenna response. This delay produced invalid correction values, increasing the first reflection response. This significant reduction in the first reflection response was measured using commercial test equipment and software simulations.

To accommodate the antenna and electronic updates, the mechanical assembly was modified to integrate all the new and redesigned components. The graphical user interface for the MSHA demonstration consists of a PDA. The original algorithm was converted for use on a PDA device. The complete LAR system except the antennas is shown in Figure 2-7. Figure 2-8 shows the two antennas (RX and TX) in a new fixed-separation chassis with adjustable tripod legs.

Figure 2-7. SDT electronics, PDA display, and battery pack.

Figure 2-8. LAR radar antennas on fixed-position tripod.

The completed LAR system was tested extensively both in the laboratory and at the Bowie Mine in preparation for the MSHA Demonstration. The salt and sandbag wall (coal seam simulant) and water-reflector (water-containers) provided a positive, repeatable response to the LAR system (Figure 2-9). The data collected at Bowie was completely analyzed to finalize and validate the algorithm before the final tests were scheduled.

Figure 2-9. Coal seam simulator at the Stolar facility (salt block and sand bag construction). Water jugs provide reflection surface.

Additional information on radar theory, LAR electrical design, and background research is given in Appendix A.

3.0 LOOK-AHEAD RADAR ANTENNA EVALUATION

3.1 ANTENNA STRUCTURES

The antenna structures designed, built, and tested for use with the SDT radar for radio geophysical applications support transmission of double-sideband ($\omega_o - \omega_1$, $\omega_o + \omega_2$) suppressed-carrier (ω_o) waveforms. Partial suppression of the first interface reflection can be achieved with polarized antennas. Additional suppression of approximately 20 dB can be achieved with circularly polarized antennas. The TX (transmit) and RX (receive) antennas must have opposite polarization—left-hand and right-hand. The following potential LAR antennas were evaluated over the course of this project:

- A pair of narrow-bandwidth resonant microstrip patch antennas (RMPA), [$\omega_o + \omega_2$] and [$\omega_o - \omega_1$]), differenced in frequency by constant or variable modulation frequency ($\omega_m = (\omega_1 + \omega_2)/2$)

- A pair of wide-bandwidth horn antennas for SFCW constant or variable modulation frequency (ω_m) and suppressed carrier stepped through the band

- A pair of fox hunter antennas (compound electric and magnetic dipole antennas) driven out of phase by approximately 90° to obtain a suppressed back lobe. A wideband sleeve dipole element is the receiving antenna.

- A pair of identically [right- or left-] hand circular polarized (XHCP) wide-bandwidth spiral antennas (for FMCW with a constant modulation frequency with the suppressed carrier sweep through the band at the rate of fs (10 KHz)

- A pair of XHCP wide-bandwidth spiral antennas (right-hand circularly polarized [RHCP] or left-hand circularly polarized [LHCP]) for SFCW constant modulation frequency ($\omega_m = (\omega_1 + \omega_2)/2$) or variable modulation frequency (ω_m) and the suppressed carrier frequency stepped through the band.

These antenna structures were evaluated in the order listed over the duration of this project. At each stage of testing, the antenna's performance for depth of penetration and sensitivity was evaluated against the LAR specifications. Unfortunately none of the three initial designs met these specifications. Ultimately, only the spiral antennas achieved the level of performance discussed in the original proposal. The spiral antennas underwent several iterations of construction and tuning before satisfactory performance was measured.

The final antenna design used for the underground demonstrations was a set of wideband spiral antennas set at a specific and fixed separation and orientation. The polarization of the transmitter and receiver antennas, relative to the coal seam and each other, also was critical to system performance and is incorporated into the mechanical construction. This polarization will be

fixed for all future coal seam operations. A brief description of the underground testing and resulting radio geophysical performance of each antenna follows.

A thin, conformal, resonant RMPA has been extensively developed for horizon sensing as described in the background patents (see Section 6). These antennas are protected by an MSHA-approved polycarbonate lens. The lens, RMPA substrate material, and the physical length of the top copper patch determine the resonant frequency. The 3-dB bandwidth is 1 to 3 percent, depending on the material used in the RMPA. A resonant standing wave pattern is excited in front of the RMPA, originating at its center conductor (input copper coaxial transmission line) and terminating along its edge. This radial distance establishes the driving point impedance for the patch. Radiation is essentially zero along each side of the patch. The length of the patch is approximately one half wavelength and depends on the effective relative dielectric permittivity of the protective lens and substrate. However, while RMPA antennas have been successful for a number of Stolar-designed coal seam sensors, their potential in an LAR application was never realized. RMPA and wide-band dipole antennas, shown in Figure 3-1, were tested at the Deer Creek Mine during this project. Lower frequency and wider band antennas were the next configurations to be evaluated.

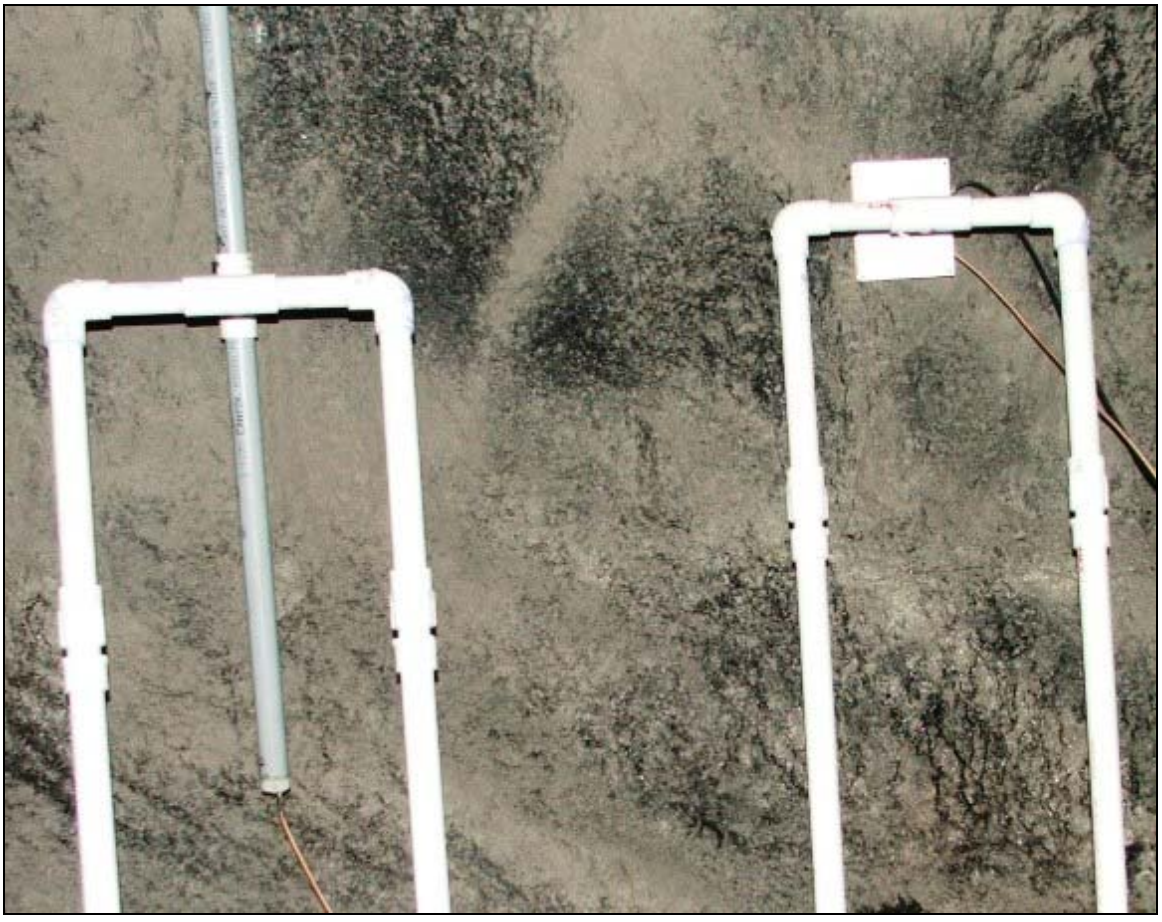

Figure 3-1. Wide-band dipole antennas (left) and RMPA antennas (right) were tested at the Deer Creek Mine. Neither antenna performed to LAR specifications.

Unlike the RMPA antennas, low-frequency, wideband dipole antennas cannot be used as transceivers. Therefore a transmitter and receiver had to be constructed. These dipole antennas initially showed enough promise that they were incorporated into a functional LAR prototype using the early version of the SDT electronics. This prototype, shown in Figure 3-2, also was tested at the Deer Creek Mine.

Figure 3-2. Low-frequency, wide-band dipole antennas were also tested with the LAR electronics as independent transmitters and receivers.

Also built and tested was a higher frequency (1-MHz) induction tool that included a high-power transmitter and a loop receiver antenna. The directivity and forward-looking sensitivity of this receiver was controlled by a copper mesh back-plate. The induction antenna is shown in Figure 3-3. This antenna also proved too ineffectual to warrant continued refinement for the LAR prototype.

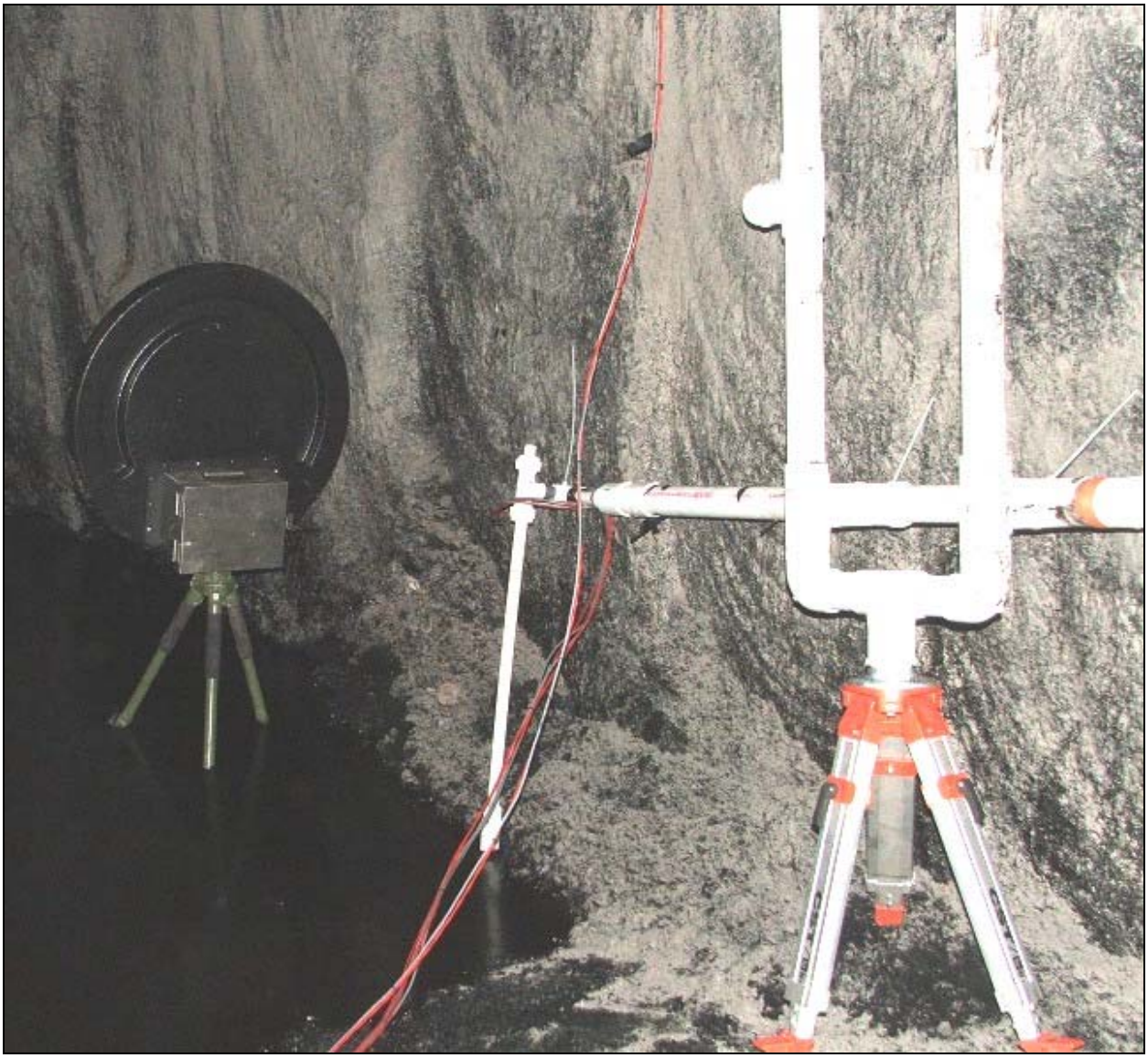

Figure 3-3. The higher frequency induction tool that included a 1-MHz transmitter and a loop antenna receiver was tested in a coal seam.

The antenna structures described in the previous paragraphs were thoroughly characterized for their performance in detecting the reflection planes in the coal seam that result from air-filled voids opposite the rib shown in the photos (actually a gate road pillar). Their typical performance is described in Table 3-1. As evident from the table, only the circular polarized XHCP wide-bandwidth spiral antennas showed any significant depth of penetration (X = R if right-hand polarized, or X = L if left-hand polarized).

Table 3-1. Radio Geophysics Applications, Suppression of First Interface Reflection.

SDT Radar Antenna	Type of Interface Radar	Range (ft)	Modulation Frequency (f_m) (MHz)	Suppressed Carrier Frequency (f_o)
LAR XHCP, XHCP	Void SFCW FMCW	20	1.54	140-240 MHz f_o = 190 MHz A = 0.12 dB/ft
HS RMPA1, RMPA2	Boundary CW, DSB	(0.82)	37.5	250-286 MHz f_o = 2.68 MHz
High wall XHCP, XHCP	Rib thickness SFCW	4	15.4	140-240 MHz f_o = 155 MHz
DSR, coal RMPA1, RMPA2	Boundary CW, DSB	3.28	18.75	250-268 MHz f_o = 2.59 MHz
[1]Phase 0 to 360° → 0 to 1.57 ft [2]Phase 0 to 360° → 0 to 1.84 ft				
DSR, limestone fox hunter	Limestone, shale CW	20	0	f_o = 1 MHz λ = 46 ft 55 dB 7.03°/ft
DSR, limestone dual horn	Limestone, oil porosity SFCW DSR	3.28	6.25	2 to 2.5 GHz α = 8.32 dB/ft
DSR, limestone dual fox hunter	Limestone, shale CW, DSB	6.0	3.42	1 and 4.42 MHz f_o = 2.7 MHz λ = 398.3 ft 9.7°/ft

CW = continuous wave
DSB = double sideband
DSR = Drill String Radar
FMCW = swept frequency, continuous wave
HS = Horizon Sensor
LAR = Look-Ahead Radar
LHCP = left-hand circular polarized
RHCP = right-hand circular polarized
RMPA = resonant microstrip patch antenna
SDT = software-definable transceiver
SFCW = stepped frequency, continuous wave

3.2 REFINEMENT OF SPIRAL ANTENNAS

The Archimedean spiral antenna showed the best performance in the LAR application testing at Deer Creek and other sites. It was decided that this antenna should be redesigned for optimal performance and matching SDT interface.

The Archimedean spiral is typically backed by a lossy cavity to achieve frequency bandwidths of 9:1 or greater. In this discussion the Numerical Electromagnetics Code (NEC) was used to simulate the Archimedean spiral. Also, several Archimedean spirals were built and tested to validate the results of the NEC simulations.

A self-complementary Archimedean spiral antenna is shown in Figure 3-4. A spiral antenna is self-complementary if the metal and air regions of the antenna are equal. The input impedance of a self-complementary antenna can be found using Babinet's principal, giving

$$Z_{metal}\, Z_{air} = \frac{\eta^2}{4} \ , \tag{3-1}$$

where η is the characteristic impedance of the medium surrounding the antenna. For a self-complementary Archimedean spiral antenna in free space the input impedance should be

$$Z_{in} = \frac{\eta_o}{2} = 188.5\Omega \ . \tag{3-2}$$

Each arm of an Archimedean spiral is linearly proportional to the angle, φ, and is described by the following relationships

$$r = r_o\phi + r_1 \ and \ r = r_o\left(\phi - \pi\right) + r_1 \ , \tag{3-2}$$

where r_1 is the inner radius of the spiral. The proportionality constant is determined from the width of each arm, *w*, and the spacing between turns, *s*, which for a self-complementary spiral is given by

$$r_o = \frac{s + w}{\pi} = \frac{2w}{\pi} \ . \tag{3-4}$$

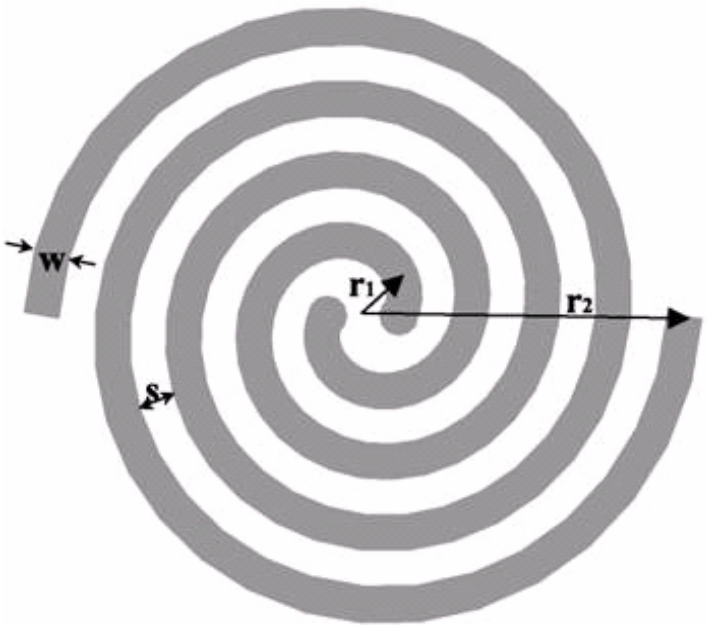

Figure 3-4. Geometry of Archimedean spiral antenna.

The strip width of each arm can be found from Equation 3-5,

$$s = \frac{r_2 - r_1}{2N} - w = w \ , \tag{3-5}$$

assuming a self-complementary structure. Thus, the spacing or width may be written as

$$s = w = \frac{r_2 - r_1}{4N} \ , \tag{3-6}$$

where r_2 is the outer radius of the spiral and N is the number of turns. Equations 3-1 through 3-5 apply to a two-arm Archimedean spiral, but in some cases four-arm spirals may be desired. In a four-arm spiral, the arm width becomes

$$w_{4-arm} = \frac{r_2 - r_1}{8N} \tag{3-7}$$

and the proportionality constant is

$$r_{o,4-arm} = \frac{4w}{\pi} \ . \tag{3-8}$$

The Archimedean spiral antenna radiates from a region where the circumference of the spiral equals one wavelength. This is called the active region of the spiral. Each arm of the spiral is fed 180° out of phase, so when the circumference of the spiral is one wavelength, the currents at complementary or opposite points on each arm of the spiral add in phase in the far field.

The low-frequency operating point of the spiral is determined theoretically by the outer radius and is given by

$$f_{low} = \frac{c}{2\pi r_2} \ , \tag{3-8}$$

where c is the speed of light. Similarly, the high-frequency operating point is based on the inner radius, giving

$$f_{high} = \frac{c}{2\pi r_1} \ . \tag{3-9}$$

In practice, the low-frequency operating point will be greater than predicted by Equation 3-8 because of reflections from the end of the spiral. The reflections can be minimized by using resistive loading at the end of each arm or by adding conductivity loss to some part of the outer turn of each arm. Also, the high-frequency limit may be less than found from Equation 3-9 because of feed region effects. The initial LAR spiral antennas are shown in Figure 3-5.

Figure 3-5. Prototype spiral LAR antennas
(TX on left, RX on right).

The circumferential length of each spiral is equal to the wavelength of the lowest frequency of the FMCW or SFCW radar (0.79 m [31.1 in.]). The radial distance (D) between fixed points is the highest frequency wavelength ($\lambda/2\pi$) of the FMCW or SFCW. The two-arm spiral design slows down the phase velocity of the traveling EM wave. The relative dielectric permittivity also slows down the traveling wave.

Once an acceptable dielectric permittivity was selected for the antennas' composition and the polarization and TX-RX separations were chosen, the final LAR spiral antenna design was selected and integrated into the system for final debugging and demonstration. The final LAR spiral antennas are shown in Figure 3-6. This pair of spiral antennas suppresses the first interface wave by an additional 20 dB; suitable for LAR applications.

Figure 3-6. Final spiral antenna configuration for demonstration field testing.

4.0 LOOK-AHEAD-RADAR FIELD TESTS

4.1 BACKGROUND

Stolar's LAR team has field tested the LAR components under actual underground mining conditions throughout the duration of this project. In all, five major testing efforts took place for various LAR subsystems and prototypes. Three of these testing efforts were experimental and were conducted for engineering reasons only; MSHA representatives were not present at these tests. The final two efforts were demonstrative and included reflection simulations, distance predictions, and observational routines designed to show LAR capabilities to one or more MSHA representatives. The data collected at these demonstration surveys also were post-processed and are presented in the following sections of this report.

Before completed LAR system testing could begin, a series of underground antennas tests were conducted at several coal mines local to Stolar's facility: the Sufco, Emery, and Bowie Mines. Tests also were conducted at Stolar's onsite salt-wall chamber. The results of these tests, summarized in Section 3, were used to refine the system design and performance specifications during the course of this project. Without being able to use these real-world testing environments, the functionality of the LAR system would never have been realized.

The two primary demonstration tests were conducted in September 2006 (Mine No. 84) and February 2007 (Bowie Mine). The results of these demonstrations are outlined in the closing sections of this report. Supplemental information on testing procedures, equipment, and mine locations is given in Appendix B.

4.2 MINE NO. 84 LOOK-AHEAD RADAR DEMONSTRATION, SEPTEMBER 2006

The early results from LAR experimental tests proved that voids ahead of mining were detectable using VHF-band predistorted EM-wave radar. However, the current LAR system requires confirmation of performance capability and limitations at an active mine site. Project partner Consol Energy identified several underground test sites near their active longwall and development operations at the No. 84 Mine near Washington, Pennsylvania. Consol worked with Stolar and MSHA to develop a strategic test and demonstration of the LAR functionality at this mine. These tests involved measuring radar reflections of air- and water-filled voids through pillar blocks to predict the thickness of the coal pillar, i.e., the predicted distance from the LAR to an in-seam reflection plane. Although the test instrumentation was used in a fresh-air environment, a temporary approval was obtained from MSHA to perform the tests because the equipment is not certified.

The overall objective of this field demonstration was to detect air- and water-filled voids in the coal seam at least 20 ft ahead of the LAR system and to quantify the performance of the LAR

system under real coal-mining conditions. Itemized objectives of the LAR testing were as follows:

- Determine the optimal in-seam radiation patterns of the TX and RX antennas
- Assess the detection performance of the RX antennas and SDT electronics
- Assess the processing performance of the LAR SDT radar software and display
- Collect transmission data through the pillar to evaluate frequency-dependant attenuation rates (signal decay and absorption rates)
- Identify operation limitations of LAR hardware, data- processing software, and antenna design.

The LAR testing took place in the active workings of Consol's No. 84 Mine. A site was selected at cross-cut #14 in Section 7B between Entries #2 and #3. This site was used for *static* testing of the LAR system through a tapered pillar with a void reflector simulant in a specially constructed chamber. The stimulant consists of a block-constructed chamber along the rib, which was flooded or drained to create either water or air reflection targets for the LAR system, which was placed against the outby rib of XC-14. The input, output, and level of the chamber water were controlled by the mine personnel.

The static LAR test site, diagrammed in Figure 4-1, was located at Chute-14 in Section 7B, many breaks outby of entry development. This crosscut was immediately inby an adjacent cross-cut (XC #13A) and at a slightly lower angle to the Entry #2 roadway. The pillar between the crosscuts was effectively tapered and ranged from 10 ft (3 m) thick near Entry #2 to nearly 70 ft (21 m) thick near Entry #3. The specially built chamber used as a void simulant for LAR reflection testing was located at the outby end of this pillar (the thinner end). All radar equipment was operated and all data were collected by Stolar personnel.

The pillar also was used to collect signal transmission data. Using the LAR system in stand-alone TX and RX modes, signal propagation characteristics were measured by broadcasting radar frequencies from XC-14, through the pillar to XC-13A. These data are critical to system calibration and optimization and aid in post-test data analysis and evaluation.

The LAR testing was performed using a combination of Stolar-built instrumentation and commercial test equipment. The power sources for this equipment were self-contained; no outside power was required from the mine operator. Descriptions of the test equipment follow along with a table of power specifications for those items that required an operating voltage.

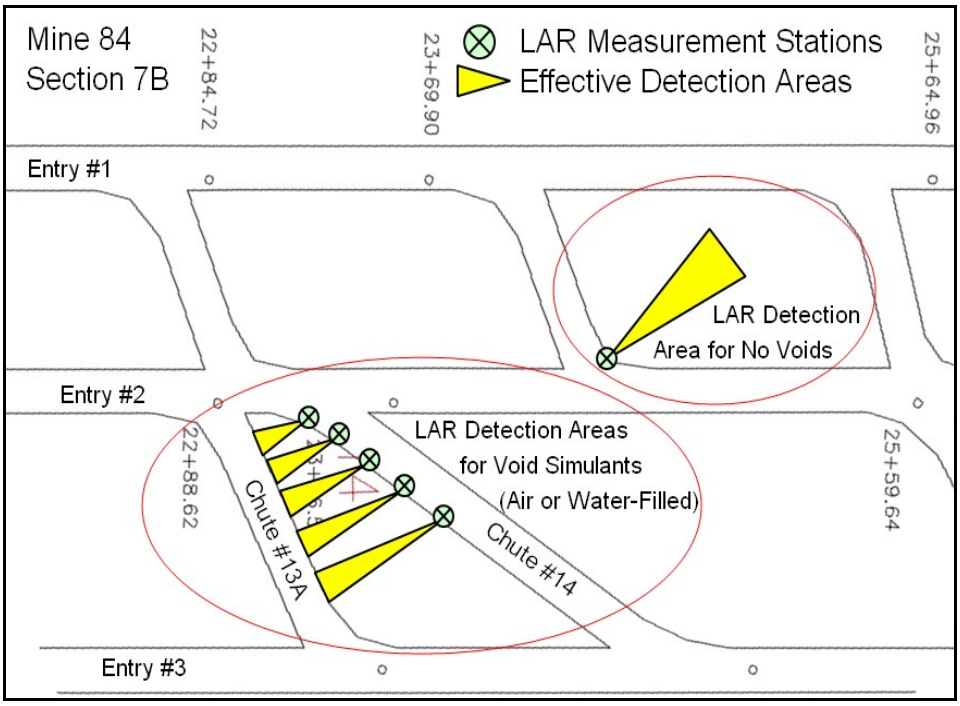

Figure 4-1. LAR static test sites: No. 84 Mine, Section 7B, Chutes 13 to 15.

The majority of LAR testing used several Stolar-built radar antennas for generating and processing reflection data from a transceiver array. The transceiver equipment consists of a TX antenna, an RX antenna, and control electronics. All components derive power from small, self-contained, VDC battery packs. Each antenna is mounted on a high-strength tripod for placement near the rib. The transceiver antenna pairs are operated by a Stolar-built electronics module. The electronics module consists of SDT circuitry and a wireless Bluetooth link. The LAR SDT electronics module is controlled by the laptop PC with a matching Bluetooth wireless link. The TX, RX, PC, and SDT electronics are shown in Figure 4-2.

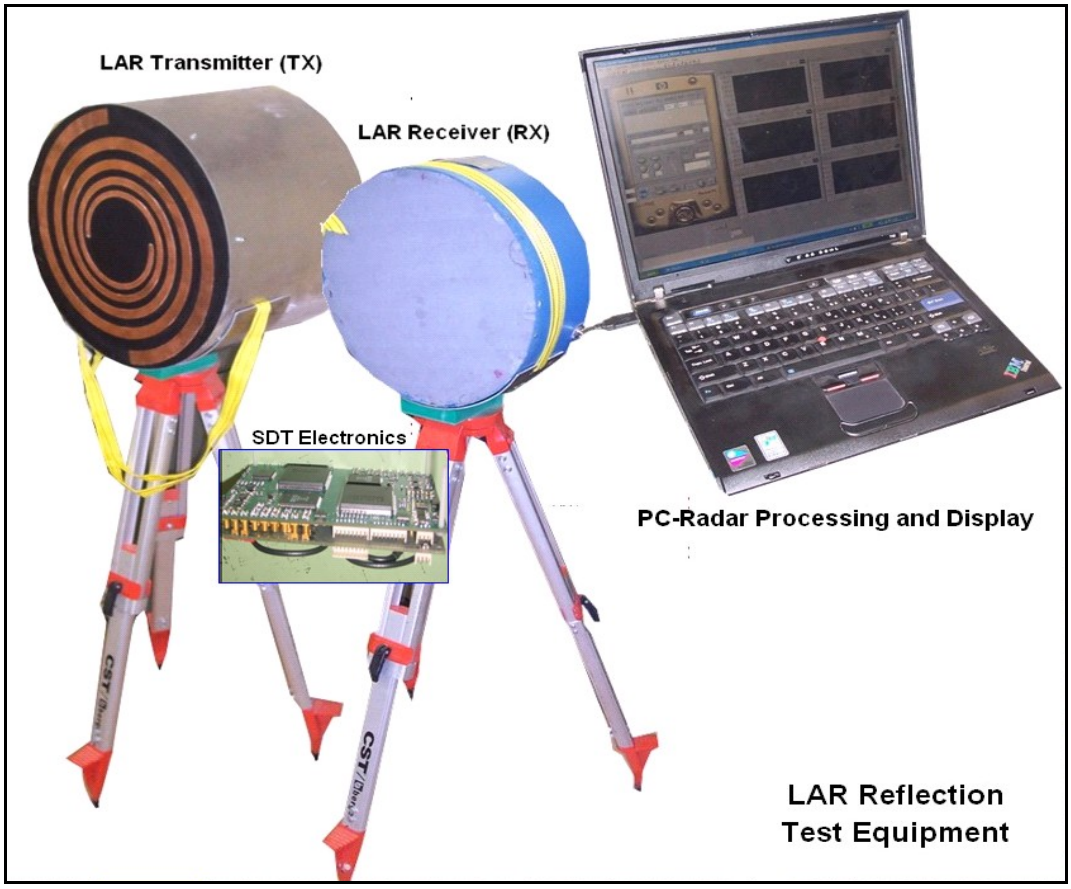

Figure 4-2. LAR test equipment (transceiver mode with PC interface).

Figure 4-3 is a representative sample of the LAR output. The correlation between LAR reflections and any of these conditions—air void, water void, no void—is poor and difficult to identify after post-processing. The noise characteristics were such that the LAR was technically working, but the signal-to-noise ratio was very low.

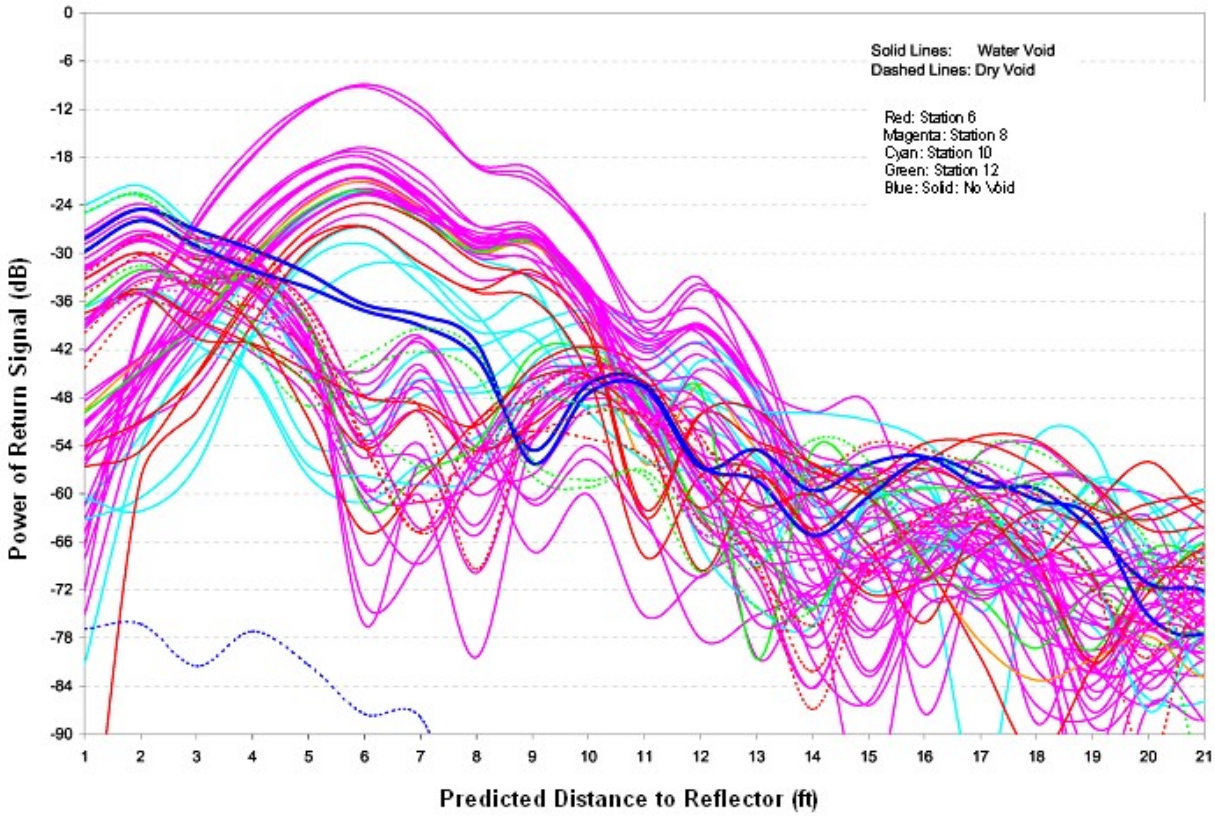

Figure 4-3. Representative sample of the LAR processed data during testing at Mine No. 84.

It is Stolar's view that the data collected with the LAR prototype at the No. 84 Mine provide evidence of radar reflection returns from the air-coal and water-coal reflector out to 20 ft. However, the return signal was weaker than expected and repeatability was poor. In assessing the state of the electronics, the efficiency of the antennas, and the quality of the spread-spectrum data sets, Stolar concluded that the LAR prototype suffered from several significant technical shortcomings. Based on these findings in September 2006, a relevant course of action for addressing these shortcomings was determined within the LAR engineering group and presented to MSHA officials in October of 2006. It was agreed at that time that Stolar would complete the system upgrades and repeat the demonstration tasks in their entirety with the finalized LAR system at another mine site. That demonstration test is reported in Section 4.3.

4.3 BOWIE MINE DEMONSTRATION, FEBRUARY 2007

The primary goal of the entire LAR project under this MSHA Void Detection Program was the field demonstration of a functional prototype system in a coal mine setting. As discussed, the initial trial at the Mine No. 84 site did not provide the results needed. Therefore, a delay in project completion was required to optimize the new LAR system based on engineering changes in electronics and antenna design late in the program. The culmination of these efforts was the demonstration tests performed at the Bowie Resources Mine on February 21 and 22, 2007.

The Bowie Mine demonstration was conducted by three Stolar representatives, an MSHA engineer from the Mine Waste Division (official observer), the Bowie Mine geologist (local project coordinator), and a CM crew. The demonstration testing was completed over two shifts, one at each of two different sites in the mine.

4.3.1 Final Demonstration Objectives

The overall objectives of the Bowie Mine field demonstration were to detect voids in the coal seam at least 20 ft ahead of the LAR system and to quantify the performance of the LAR system under real coal-mining conditions. These voids were actually the ribs of the mine's entries on the opposite sides of several pillars, both completed pillars and pillars under development. The specific objectives of the LAR tests were as follows:

- Assess the processing performance of the modified LAR-SDT radar software and display
- Collect reflection data through the pillars to evaluate the LAR depth of penetration, coal seam attenuation, and dependency of reflector type (air or water)
- Identify hardware, data-processing software, and antenna design operational limitations
- Demonstrate system operation and performance to an MSHA representative.

4.3.2 Final Demonstration Location

The final LAR demonstration took place in the active workings of the Bowie Mine. As shown in Figure 4-4, two sites were selected: a pillar at the corner of the B-6 tailgate and the 1st North Mains (preselected location at the mouth of B-5 headgate) and a cross-cut driven during production of the B-5 headgate (the exact location was determined on the day of testing).

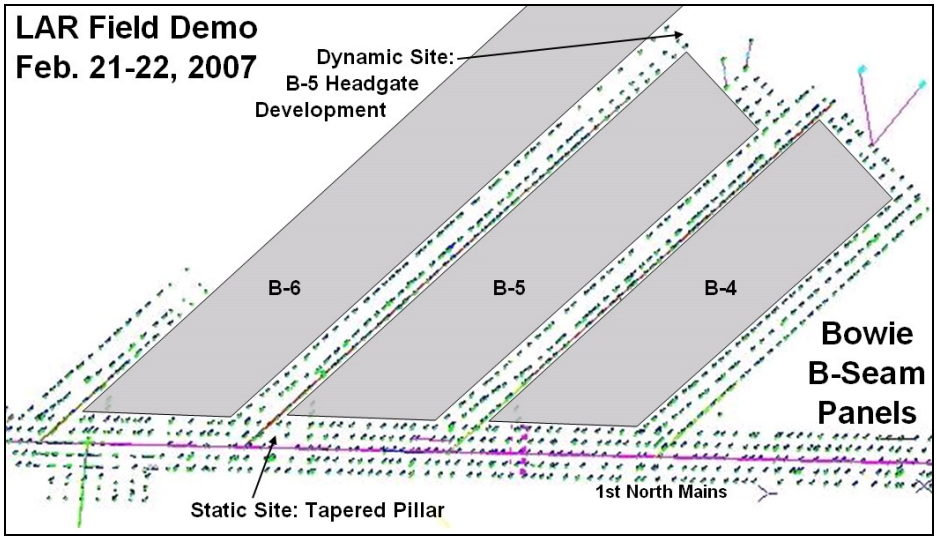

Figure 4-4. LAR test sites in the Bowie Mine upper B-Seam panels.

The first area was used for *static* testing of the LAR system through a tapered pillar where void reflector simulants were in a static position while the LAR system moved to different locations along the opposite rib to create changes in radar reflection distance. The second site was used for *dynamic* testing of the LAR system in which a pillar's width (radar reflection distance) was dynamically changed through active cross-cut development by a CM. The LAR instrumentation used, data collection procedures, and analysis of tests results for this demonstration are described in the following sections.

4.4 LAR DEMONSTRATION SYSTEM

The LAR system uses portable, self-contained radar antennas to generate and process reflection data from a transceiver array. This array consisted of a TX and an RX antenna connected with an optimal antenna orientation. Reflection tests involved using the TX and RX units fixed side by side to measure the distance to a reflecting boundary within the coal seam (opposite side of pillar). The antennas were driven by the LAR SDT electronics module and controlled by the laptop PC. All components derived power from small, self-contained VDC battery packs. The antenna array was mounted on a high-strength tripod for placement. The LAR transceiver was typically within 1 ft of the pillar rib during data collection. The TX-RX array, control PC, and LAR-SDT electronics are shown in Figure 4-5.

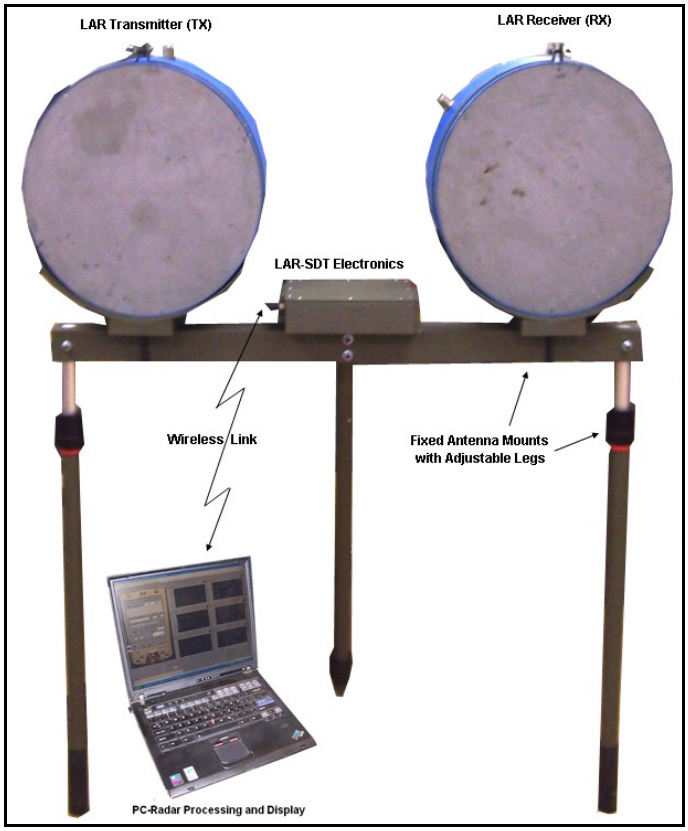

Figure 4-5. LAR transceiver array with PC interface to SDT (via wireless PC link).

The operation control and visual graphics provided by the laptop PC are actually a simulation of a PDA-designed software application. For the purposes of the demonstration, the PC was used in lieu of the PDA so that supplemental data processing and storage applications could be used to better evaluate and record the large volume of radar data in real time over a conceivably long period of time. The display screen and iconic controls of the PDA are shown on the PC screen as an emulation of the LAR's actual functionality.

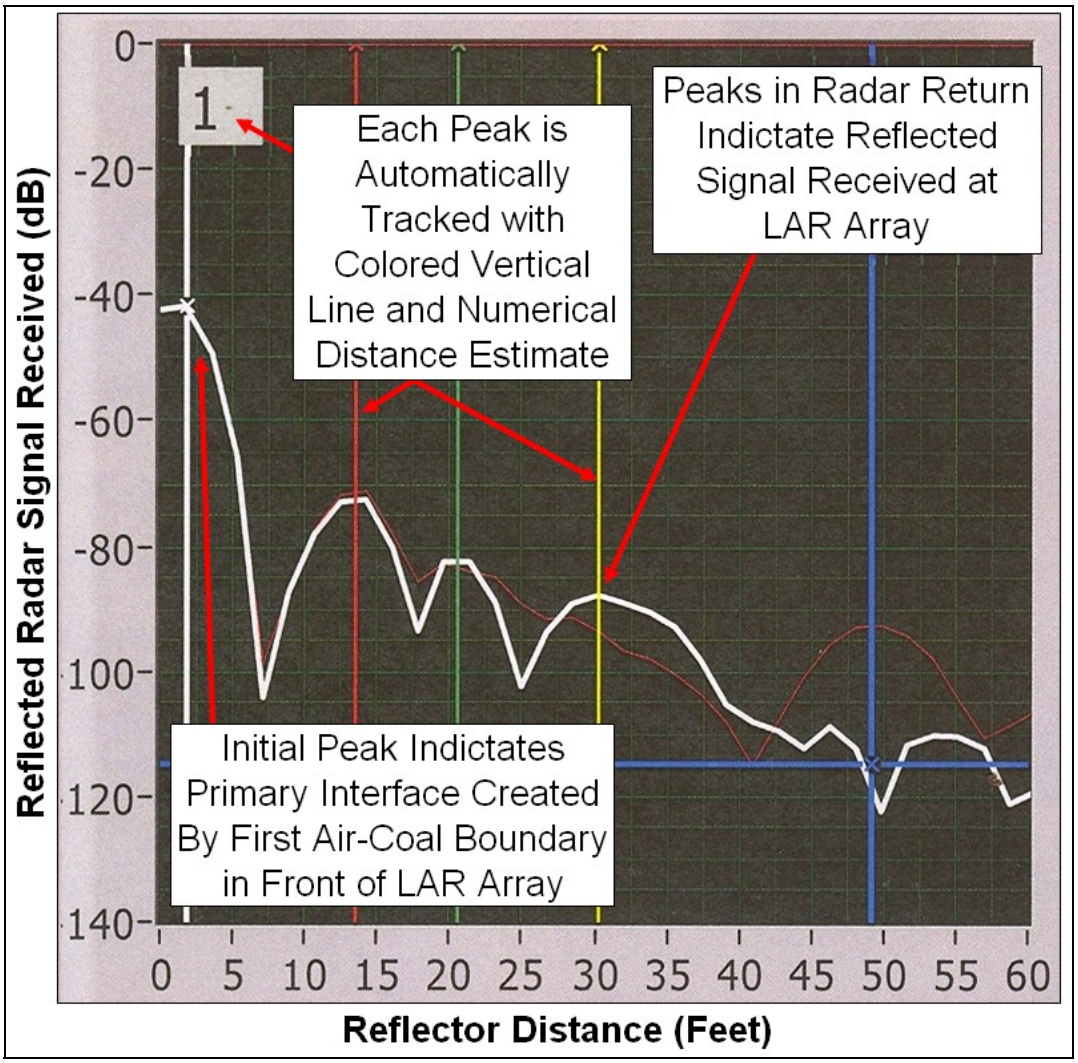

Figure 4-6. LAR display screen and iconic controls of the PDA interface produced on the PC screen via a custom demonstration application.

The LAR display, shown in Figure 4-6, shows the peaks in the radar's return signal if received above the system noise at that distance. Each reflection peak is automatically tracked with a colored vertical line if it satisfies a minimum magnitude threshold (blue horizontal line) relevant to the background. A numerical position is estimated at this distance and shown on the screen. The reflection surfaces surrounding the LAR also are seen in the display, including the primary interface created by first air-coal boundary in front of the LAR array and the structures directly

behind the array. These reflection peaks in the return signal are consistent and stationary on the display. Reflections associated with a void interface through the coal seam will track up through the distance axis as the LAR array moves towards the interface. Each sharp reflection is identified by a colored vertical line and the distance to this reflection peak is displayed on the screen in units of feet. A distance threshold (blue vertical line) is also established to limit the region within which the software will identify sharp reflection peaks. In addition to displaying the current radar profile (heavy white curve), the display also shows the previously recorded profile (light red curve). Reflections that have not moved from one measurement to another will be obvious because the peaks from the white and red profiles (amplitude and distance) will be similar and therefore overlap. These reflections can be considered fixed relative to the LAR unit and are generally near-field reflections such as the entry walls and equipment in the area of the antennas. Moving reflection planes will be indicated as peaks that shift between the white and red profiles.

The horizontal axis represents the predicted distance from the LAR receiver antenna to the signal reflector. This predicted distance is the quotient of the radar-estimated reflection distance and the square root of the assumed dielectric constant (or relative dielectric permittivity). While the original scope of work suggested that the LAR system could measure the in situ dielectric constant in real time, this functionality was not realized in the prototype before the final field testing. Therefore, during all LAR field testing, this dielectric constant was assumed to be 6.5 (an average value for most coal seams).

The vertical axis represents a logarithmic scale for return signal power. A 0-dB level is calibrated to equal the power of the transmitter (before antenna radiation). The -40-dB level is the y-intercept of the return signal (distance equals zero). This is essentially the radiated power of the transmitter antenna. This 40-dB drop in signal level from the input to the output of the transmitter antenna represents the antenna's inefficiency. This -40-dB level can be considered the coupling factor of the radiation, i.e., that power actually entering the coal seam at the initial air-coal boundary.

Testing at all Bowie sites involved only reflection testing using the LAR prototype. Unlike during previous tests, no transmission testing or commercial test equipment were required at the Bowie Mine for the final demonstration. The LAR system runs entirely from small self-contained VDC battery packs. These packs provide 12 to 15 VDC at current levels below 2 A. All battery packs are sealed and fuse protected. No outside power was required from the mine.

4.5 DATA COLLECTION AND RESULTS

4.5.1 Static Test Data Collection and Results

The static LAR test site was located at Cross-Cut #52 in Entry 5 of the 1st North Mains. This area possesses a roadway developed at an angle to the main entries. The outby-most pillar thus formed a tapered shape through which increasing coal thickness can be measured as the LAR system moved inby along the pillar rib. This taper effectively created reflection distances ranging from 10 ft to nearly 40 ft. The total signal propagation distances would be double these ranges (incident outbound and reflection return signal travel).

All the LAR equipment operation and data collection were performed by Stolar personnel with the logistical assistance of MSHA and Bowie representatives. This pillar was entirely in fresh air and the LAR system was used exclusively in the roadway of the Mains. The opposite roadway consisted of the headgate beltway as a "void" simulant. The rib of this entry was used to create reflection surfaces. The reflection planes themselves consisted of the open rib (air-filled void) and a collection of water-filled plastic containers (water-filled void).

The water-reflector was far from optimal in terms of realism, scale, and scientific validity; however, this was a compromise between demonstration requirements and mine site logistical capabilities. The construction of a water-filled chamber, like that used at Mine 84 in a previous field exercise, was not possible given the schedule and budget constraints for the final demonstration. The collection of water-filled containers was stacked as a block wall against the headgate rib. These containers were filled with moderately saline water to create a water-reflection target for the LAR system through about 20 ft of coal in the pillar.

During data collection at the static test site, radar signals were propagated through the coal pillar at three discrete measurement stations while the PC processed and recorded reflection data. Each station represented increasing coal pillar width (A = 10 ft, B = 20 ft, and C = 30 ft). This procedure is diagrammed in Figure 4-7, which also shows the sequence of data collection for the static test site.

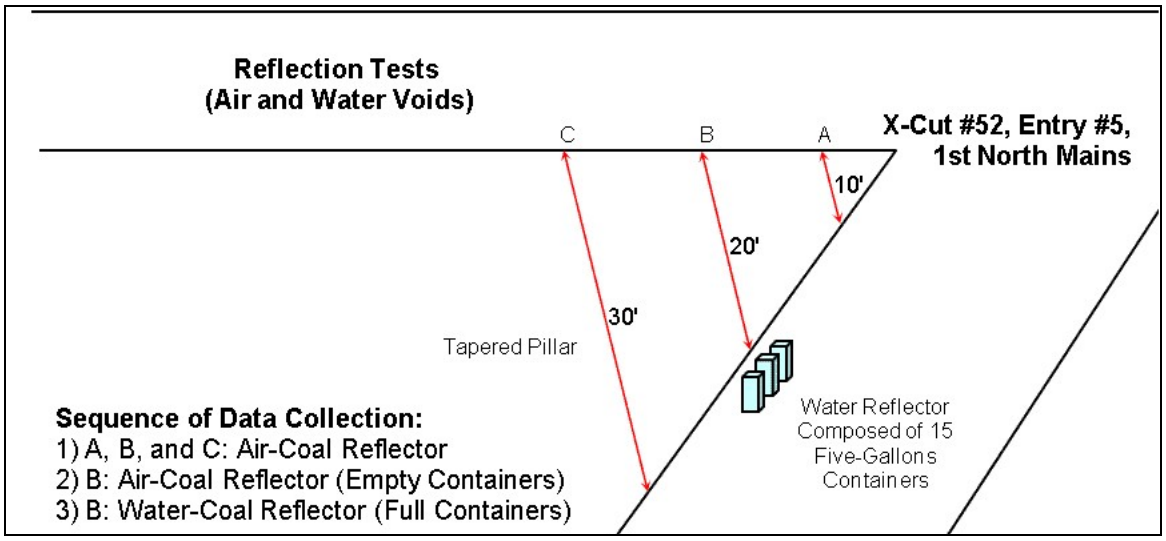

Figure 4-7. LAR *Reflection* test diagram, static test site.

As described, the water-coal reflection interface was simulated using 5-gallon water containers placed along the rib. This wall of 15 water containers was approximately 5 ft wide, 5 ft tall, and 6 in. thick. This water-reflector constituted only 75 gallons of water, but was a practical size to manage for the mine site on short notice. The data collection process was repeated at the 30-ft thickness station 3 times with the following interfaces as the reflecting surface:

- Simple air-coal boundary (open rib)
- Air-coal boundary with empty water containers

- Water-coal boundary with full water containers.

The LAR prototype system setup in the 1st North Mains Entry for the Static Testing is shown in Figure 4-8. The headgate rib used as the reflecting surface for these tests is seen in Figures 4-9 and 4-10, for the air-coal interface (with empty containers) and water-coal interface (with filled containers), respectively.

Figure 4-8. LAR prototype system in place against rib at Bowie Static Test Site, February 21, 2007. The transceiver array was placed at several locations moving inby down the rib for data collection through increasingly thick coal seam (on tapered pillar).

Figure 4-9. An open rib in the B-5 roadway provided an air-coal reflecting surface through the tapered pillar at Bowie Mine static test site.

Figure 4-10. A water-coal interface was created on the rib using plastic containers filled with moderately-saline water. The containers created a small reflecting wall opposite of the LAR system at the 20-ft thickness station through the pillar.

The results of the static testing at Bowie were mixed. In general, the LAR did predict the thickness of the coal pillar at the B location. However, the state of the rib was too deteriorated near the A location (at the corner of the taper) to provide good data. Also, the steel mesh on the ribs proved to be too strong a reflecting surface and all of the reflections simply indicated the distance from the LAR unit to the wire mesh on the opposite side of the pillar. The plastic containers were not detected in either the air-filled or water-filled data sets. These tests did allow for the relative dielectric permittivity variable to be empirically estimated at approximately 6.5 and they provided proof that the 20-foot range was achieved in the Bowie Coal Seam.

The only technical failure that occurred during static testing was that the chassis of thetripod frame on which the LAR antennas were mounted fractured and was removed from service. A temporary wooden frame was constructed between the first and second day's effort.

4.5.2 Dynamic Test Site Data Collection and Results

The dynamic test site was set up in a developing cross-cut area that was active on the day of testing. The exact location was determined within hours of testing based on that shift's production schedule. Therefore, the site selected was arbitrary and no LAR experimentation or coal seam characterization had been done at this site. However, testing at the static site the day

before did provide the LAR team with an opportunity to refine system performance and select an appropriate dielectric permittivity for the radar algorithm.

Personnel in the two adjacent entries coordinated the LAR system operation against the rib directly in front of the planned crosscut development by a CM. Thus, the pillar's width was reduced dynamically through active CM mining while the LAR system collected reflection data from the advancing mining face. Although the LAR instruments were immediately against the rib in front of the moving miner, the operating and observing personnel were about 50 ft outby of this location. This arrangement was made possible by the wireless data link between the PC and the LAR SDT electronics.

The LAR system was set up using the same TX-RX array used at the static site. The only significant changes in the system between the first and second test sites were the fabrication and use of a temporary wooden antenna frame mentioned earlier. In addition, some refinements were made to the radar software algorithm, including the relative dielectric permittivity variable. Again, the LAR transceiver was placed within 1 ft of the entry rib opposite the CM development. Radar signals then were propagated through the coal pillar at a single discrete measurement station (central to the oncoming cross-cut) and the PC processed and recorded reflection data throughout the duration of the cross-cut development via manual operation by a Stolar engineer. In total, 50 data sets were recorded during the dynamic site testing. All radar data were time stamped for later comparison with known miner position and mine face geometry. This time-dependent correlation provided accurate characterization of LAR response as functions of pillar thickness [d(t)] and CM position [x(t)], important because the CM itself was a significant reflector for the radar signals. A diagram of the dynamic test site is shown in Figure 4-11.

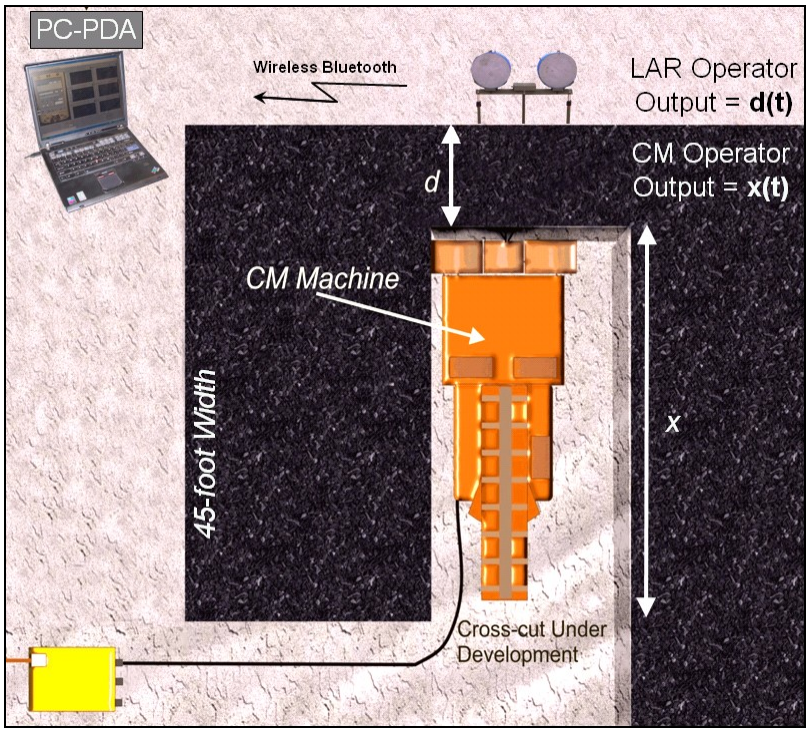

Figure 4-11. Dynamic cross-cut *break-through* test site

Coordinating this effort involved the LAR operator maintaining periodic communication with observers at the face in the opposite entry. These observers recorded mining face position and CM location as a function of time. Face position was used to calculate the actual reflector distance and the CM location was used to assess the effects of spurious reflections in the processed data resulting from the inconsistent orientation and geometry the CM body. In addition, the CM operator periodically backed the miner away from the mining face so reflection data could be recorded without these spurious reflections overlapping the reflection resulting from the freshly mined face. The LAR prototype system setup in the B-5 Headgate Entry for dynamic testing is shown in Figure 4-12. The rib in the adjacent entry is used as the reflecting surface (initially a 45-ft distance).

Figure 4-12. LAR prototype system used at Bowie Mine dynamic test site, February 22, 2007.

The most critical period of the dynamic test was just before the CM broke through the pillar into the entry. A predetermined cut depth was identified as a point at which the test equipment would be removed from the pillar and testing personnel moved away from the last open crosscut. This cut depth was intended to be 10 ft of coal seam left between the mining face and the emplaced LAR system. However, vibration on the ribs created some rib instability at about the 20-ft marker, resulting in rib coal and rock sluffing out into the entry and onto a section of the tripod holding the LAR antenna array. At this point the CM was halted, the LAR instrumentation was removed, and the demonstration discontinued. The actual LAR system was not damaged and no safety incidents or injuries occurred. The cut-through finished as scheduled and the dynamic data had been collected between the 20- and 45-ft reflection distances.

The initial measure of system performance is seen when comparing the LAR radar response as a function of reflector type and distance. The LAR response, as previously described, includes the reflection points (return signal peaks) along the distance axis of the PC's simulated PDA display

screen. This is a real-time indicator of predicted coal-seam thickness provided during underground demonstrations. These indicators were described to Bowie and MSHA observers during the final demonstration. The LAR display images shown in Figures 4-13 through 4-17 are the actual data files recorded during the dynamic cut-through. A description of the estimated reflection peaks, actual reflector interface positions, and CM location follows each image.

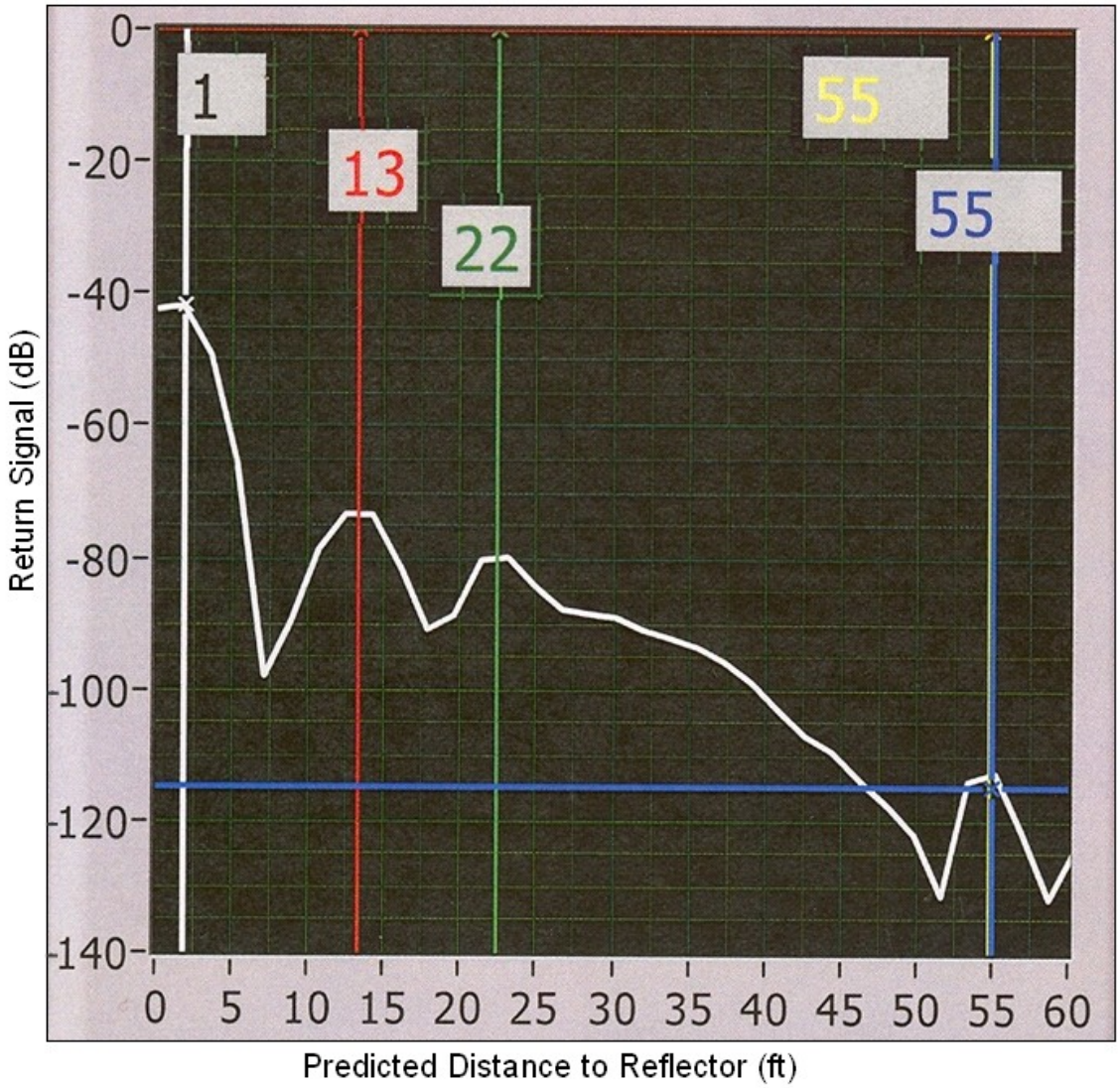

Figure 4-13. LAR display of dynamic site background reflections before mining.

Figure 4-13 shows the reflection conditions before the start of the cut through, i.e., the background reflectors. The starting thickness of the pillar was 45 ft. The white, red, and green cursors (with 1, 13, and 22-foot markers) represent static reflection peaks that exhibit the same position on the distance axis and the same signal strength on the decibel axis on all subsequent images. These static reflecting planes are the entry walls within which the LAR system was placed. These peaks can be minimized, if not entirely eliminated, with better near-field suppression and proper back-plane grounding to provide more forward-looking directivity.

These are both basic engineering efforts required in the next iteration for a commercial version of the LAR. The peak at the 55-ft mark (indicated by the yellow and blue cursors) is beyond the starting air-coal interface. The peak is consistent with the location of the CM in position before the cut.

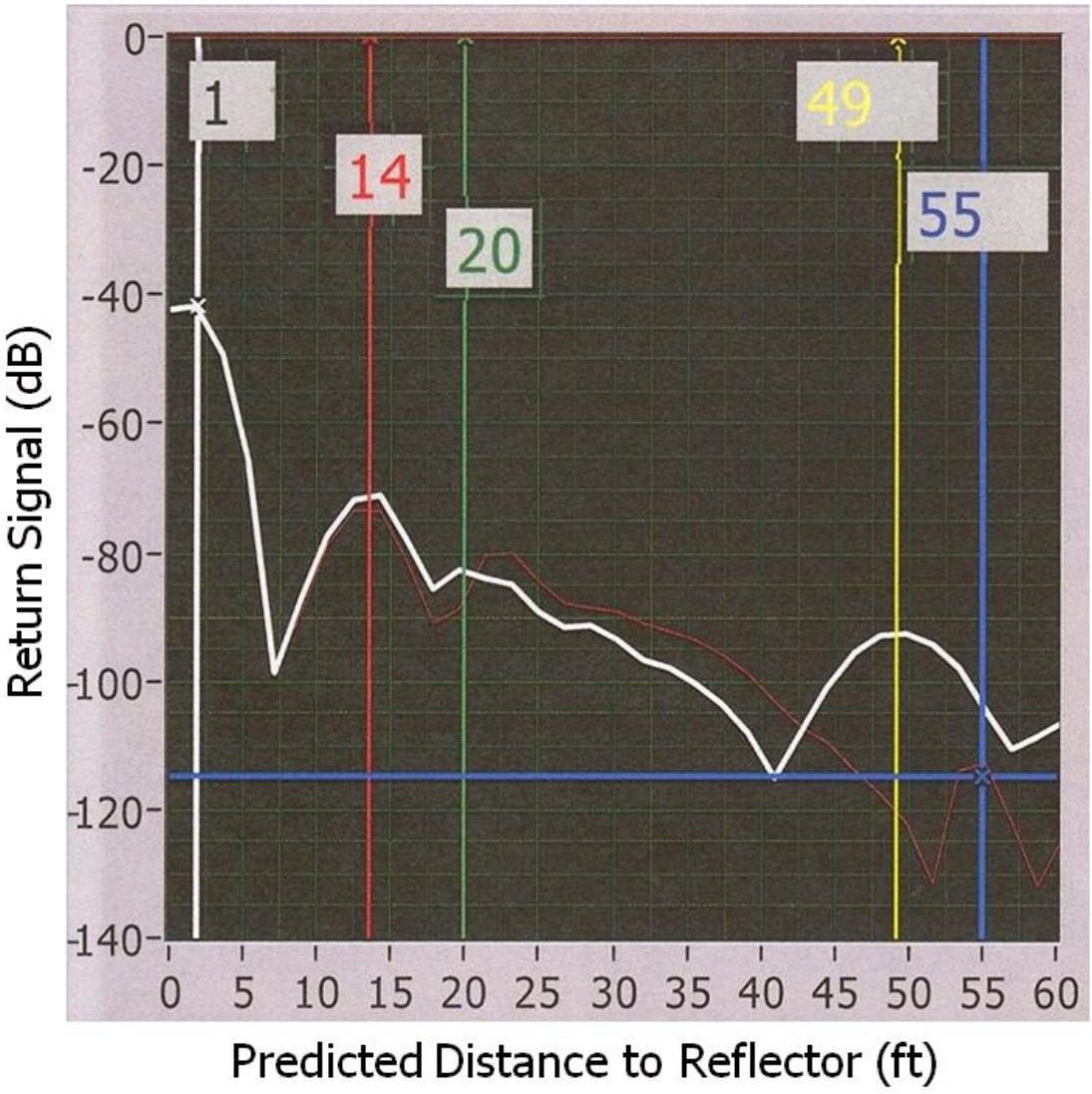

Figure 4-14. LAR reflections as CM begins to engage the mining face as the crosscut begins.

As the CM begins mining into the pillar, the reflection conditions become variable and complex. Figure 4-14 shows the reflections as the CM engages the pillar in an orientation not perpendicular, but at a low angle to the rib because its length far exceeds the width of the entry. The prominent peak indicated by the yellow cursor at 49 ft is the CM as it has moved into position to start the cut. The blue cursor marks the position that the yellow cursor held in the previous image (Figure 4-13). The cursor positions in this figure provide evidence that the CM not only affects the LAR response in this test, but that the stationary peaks created by the entry

walls near the LAR array remain constant. At this point, the CM is angled into the cut and does not present a flat, perpendicular reflection interface for the incident radar signal. Variations in the orientation of the CM in the crosscut present different radar cross sections from the LAR. This phenomenon was seen throughout the dynamic testing; only the ribs, including the approaching mine face, remain consistent and accurately predicted on the distance axis.

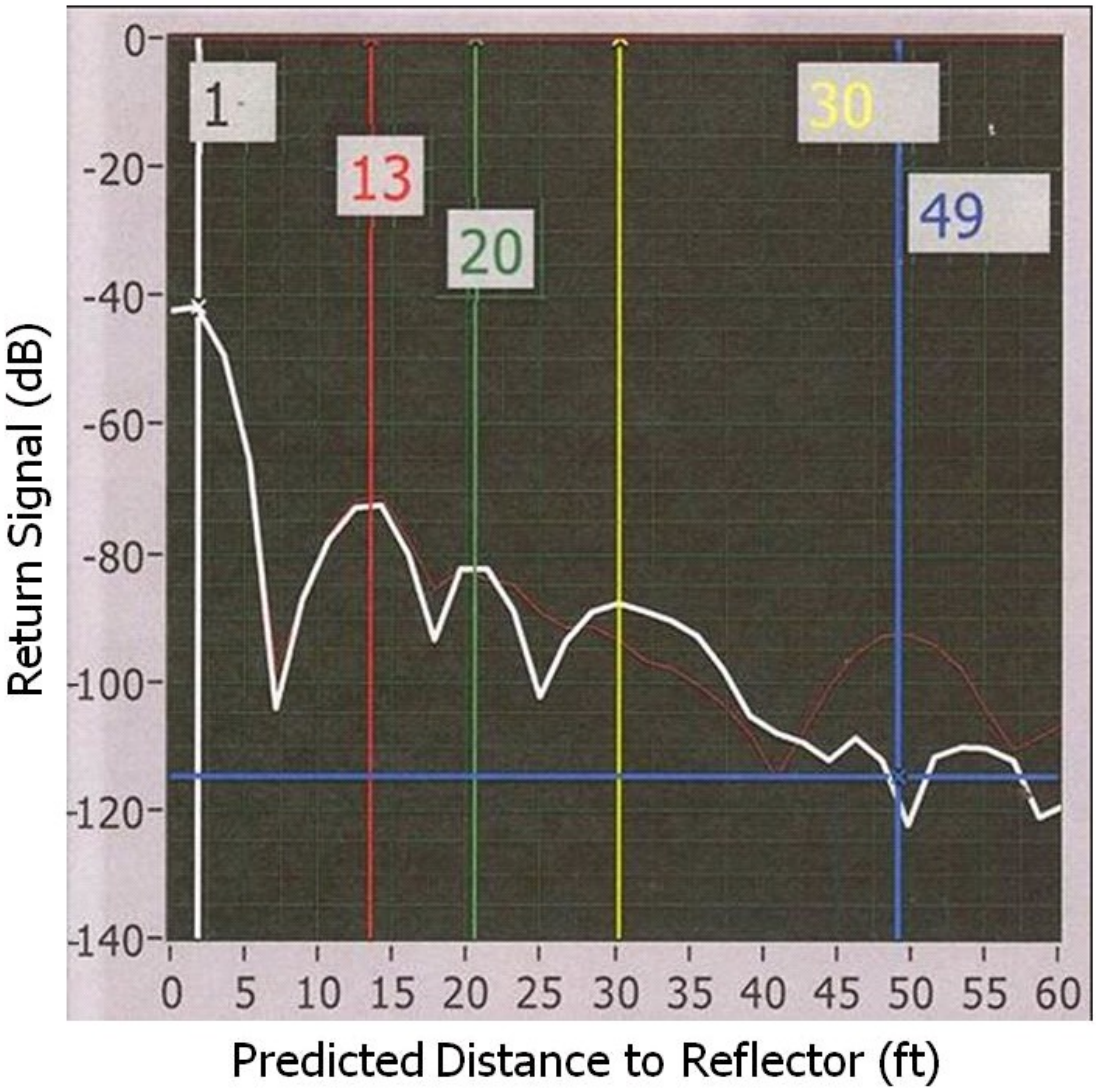

Figure 4-15. LAR reflections during active mining to a distance 30 ft from the LAR array. The peak marked by the yellow cursor is combined reflective source of the mining face and the CM.

Figure 4-15 shows the reflection conditions as the CM is actively mining coal at 15 ft into its cut-through; this places the mining face 30 ft from the LAR. This reflection distance is predicted by the LAR system and is easily identified in the display as the prominent peak marked by the yellow cursor. The depth of the mining cut at this point is the distance from the blue to the yellow cursor, supporting the validity of the reflection. However, the detected "target" at the

30-ft distance in this figure is the cumulative reflecting source made up of the mining face and the CM. This is not only a logical conclusion, but is supported by the large magnitude of the response (in decibels), which is nearly as strong as the stationary reflection off the rib behind the LAR array at the 20-ft green cursor. Only when the miner stops and is withdrawn from the face, is the validation of the mining face reflection determined.

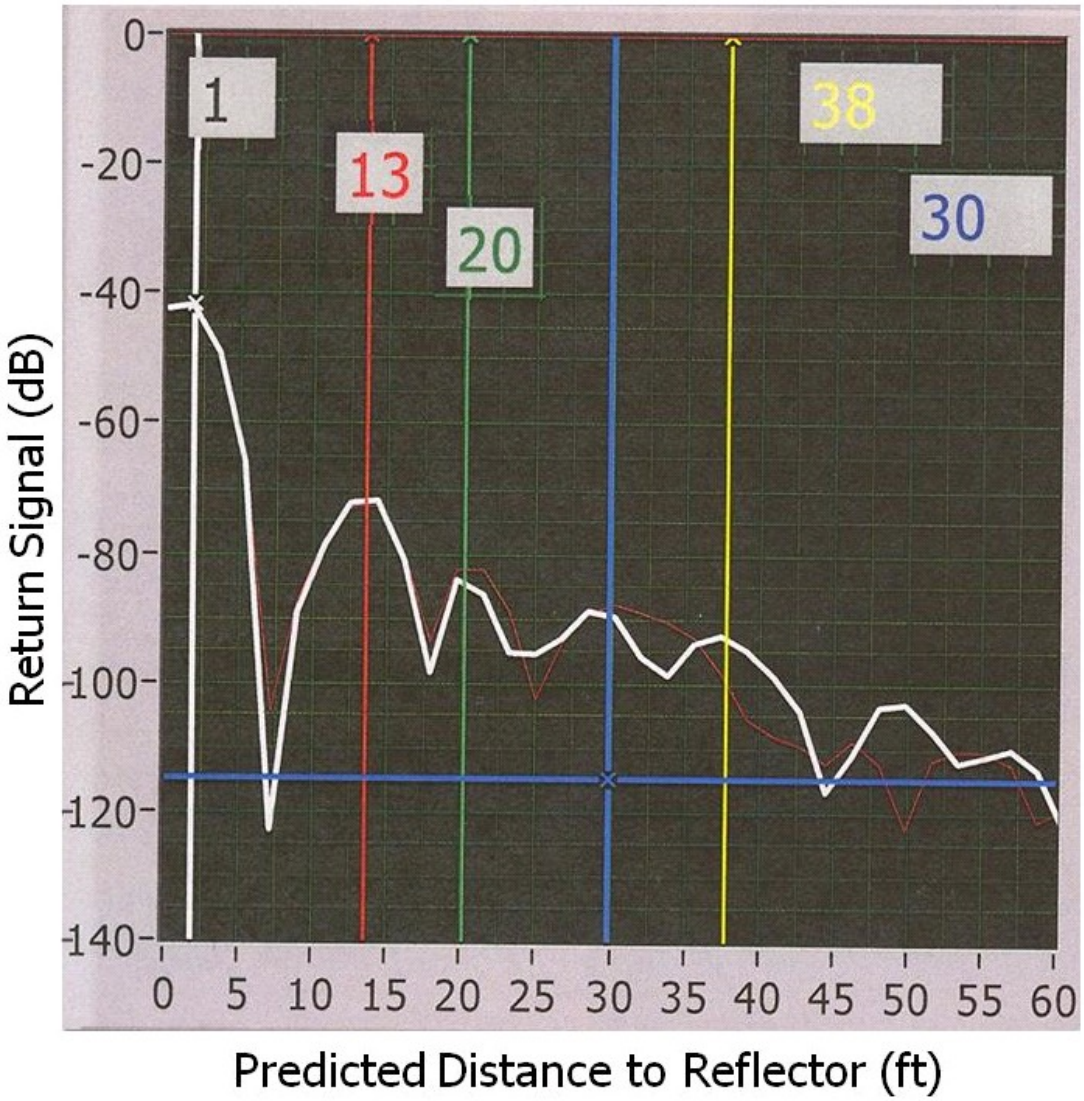

Figure 4-16. LAR display of a true air-coal reflection at the 30-ft distance marker. The mining face was established at this position and the CM was backed away (38-ft reflection). The face reflection (blue cursor) results entirely from the mining face.

The most important graphic in this entire report, Figure 4-16, shows the reflection conditions as the CM is trammed as far back as possible from the mining face. The mining face known to exist at a distance of 30 ft from the LAR remains an obvious reflection plane in the display and the position of the CM is confirmed by the secondary reflection at the 38-ft marker. The fact the

CM is not compounding the reflection characteristics of the mining face is evident by the reduction of the 30-ft peak's overall width and magnitude from that shown in Figure 4-15. The peak at 50 ft is the coal buggy.

This graphic is positive proof that the air-coal interface of the freshly cut mining face is detectable by the prototype LAR system, even with the false positives created by the stationary peaks of its local reflectors in the near field. The air-coal interface is not augmented by water, roof bolts, or mining equipment; also it is a fairly narrow reflector (crosscut width) compared to the reflecting interface that would be created by an entire entry, as seen in side view. In addition, this 30-ft detection distance is 10 ft beyond the initial objective of the program (20-ft standard). This is not to imply that 30 ft is the maximum capability of LAR in this coal seam, but rather the distance immediately supported by the logistics of this testing scenario and the limitations of the procedure during the dynamic site demonstration.

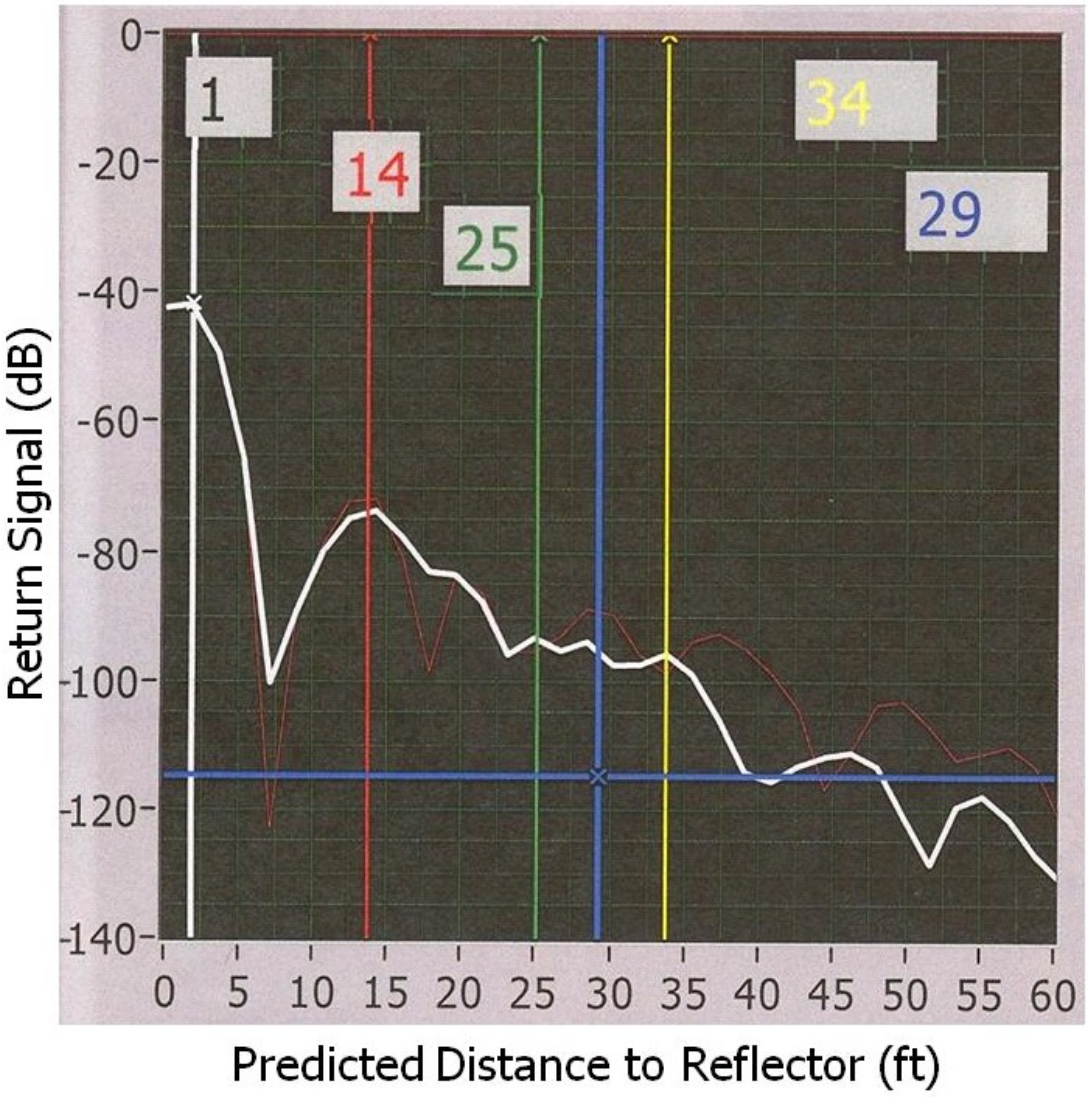

Figure 4-17. LAR Display of air-coal reflection at the 25-ft distance marker (green cursor). The CM is pushed back away from the face (28-ft reflection).

Following the positive face-reflection at 30 ft, the CM reengaged the face and progressed an additional 5 ft into the crosscut. Once a mining face was established at a distance of 25 ft from the LAR array, the CM was again trammed back away from the freshly-cut face. Figure 4-17 shows the reflection conditions with a mining face at about 25 ft and the CM pointed straight into the cut, but backed out to about the 29-foot marker. The peaks at 28 and 34 ft represent the CM. Unfortunately, the face reflection peak is beginning to overlap with the closer, stationary peaks created by the ribs in the LAR's entry. The peaks previously seen at the 13- and 20-ft markers are beginning to change shape and the magnitude of the face reflection is becoming masked by the broadening resultant peak. Some additional mining was attempted after these data were captured, but the rib in front of the LAR array caved, damaging the wooden antenna frame and stopping the test.

5.0 CONCLUDING REMARKS AND RECOMMENDATIONS

Our national goal of achieving energy independence and combating terrorism will require increasing coal production by 46 percent from the 2003 production baseline by 2025. Because easy-to-mine coal reserves are nearing exhaustion, future mining will be in deeper, thinner, and more geologically complex reserves near abandoned mines. The Quecreek Mine inundation and the report (4) from the follow-on study commissioned by Pennsylvania's then Governor, Mark S. Schweiker, recommended developing abandoned-mine detection technology. Although drilling ahead of the face is an effective method of void detection, an LAR device, once trialed, ruggedized, and made commercially available, could offers a cost-effective means of also detecting abandoned gas well pipes and mines immediately ahead of mining. The recent escalation in coal-bed methane production is emplacing metal casing at a very high rate, spoiling many of these mineable reserves. From an ignition safety and inundation point of view, it is imperative that the LAR design be transitioned from man-portable instrumentation to real-time drum-mounted instrumentation.

Stolar's LAR technology development and in-mine trials goals were established by the MSHA technical team. First, a man-portable LAR was to be developed in this project to enable the customer to provide user feedback and determine the void detection limitations. Second, the design had to be in reach of real-time operation from a cutting drum. This latter goal was to be accomplished in a follow-on project. Although a "hand-held" version of the radar was the initial objective of the program, the ultimate size of the antennas left the LAR system as merely "portable." With an antenna redesign Stolar feels that both hand-held and machine-mounted versions are within reach.

The LAR development required a significant breakthrough in the existing GPR state of the art. Radio geophysics dominates this detection problem. The detection of metal casing and voids at distances of at least 20 ft ahead of the CM requires suppressing the EM wave from the first interface by a factor of at least 40 dB because the attenuation rate is near 1 dB/ft. Stolar achieved a breakthrough in the state of the art during this project by developing an SDT capable of predistorted waveform transmission. The outstanding feature is that the predistorted waveform corrects for the frequency response of the signal path and provides first interface reflection suppression of 100 dB as measured in the laboratory. Suppression exceeding 40 dB will extend the detection range well beyond the current goal of 20 ft.

The radar return demonstrated that the CM could be tracked as it mined through the crosscut. Resolution was high enough to detect the recently cut face, leaving the uncut fender, and the backup mining machine.

The LAR firmware and software feature in-application programming, enabling improvements in instrument functionality to be made by wireless Bluetooth transmission from a PDA or a notebook computer.

The entire design can be made using the already-approved battery protection circuit.

An engineering review of the LAR and the most recent in-mine test data found that antenna back-lobe suppression needed to be improved in the commercial version of the LAR. The spiral antenna design needs improved absorption material backing the antenna along with a balanced-to-unbalanced matching network. This improvement will suppress the two reflections seen in the acquired data. The transmit power needs to be increased from 0 dBm (1 milliwatt) to 20 dBm (100 milliwatts) to enable greater detection.

A preproduction lot of three LAR systems, to be funded as a separate effort, should be manufactured and placed in a baseline test program.

6.0 REFERENCES AND BIBLIOGRAPHY

1. Domenici, Pete V., with Blythe J. Lyons and Julian J. Steyn, 2004, *A Brighter Tomorrow, Fulfilling the Promise of Nuclear Energy*, Rowman & Littlefield Publishers, Inc., Lanham, Maryland; Boulder, Colorado; New York, New York; Oxford, England.

2. Anderson, R. N., 1998, "Oil Production in the 21st Century," *Scientific American*, (March) pp. 86-90.

3. Mowrey, G. L., 1991, "Promising Coal Interface Detection Methods," Min. Eng., v. 43 (January), pp. 134-138.

4. Ramani, R.V, W. Harbert, F.R. Kirby, J.L. Kohler, S. Kravits, J. Lamont, J.S. Roberts, D.L. Smith, and J.J. Szalankiewics, 2002, Commission on Abandoned Mine Voids and Mine Safety, Report to Mark S. Schweiker, Governor of Pennsylvania, Philadelphia, Pennsylvania.

5. Chang, D. C., 1971, "Characteristics of a Horizontal Antenna Over a Dissipative Half-Space," *Technical Report. No. 4 under NOAA Grant No. E22-58-70(C)*, Department of Electrical Engineering, University of Colorado, Boulder, Colorado.

6. Monaghan, W. O., M. A. Trevits, T. P. Mucho, and J. Wood, "Geophysical Technologies for Detecting Underground Coal Mine Voids," presented at *Geophysical Technologies for Detecting Underground Coal Mine Voids*, Lexington, Kentucky, July 28-30, 2003.

7. Chang, D. C., 1973, "Characteristics of a Horizontal Loop Antenna Over a Multi-Layered Dissipative Half-Space," *IEEE Trans. Antennas Proc.*, Vol. AP-21, pp. 871-873.

8. Chang, D. C, and J. R. Wait, 1977, "An Analysis of a Resonant Loop as an Electromagnetic Sensor of Coal Seam Thickness," *URSI Conference on Propagation in Non-Ionized Media*, LaBaule, France, 18 April-6 May, 1977, pp.141-146.

9. Umashankar, K. R, D. R. Wilson, and R. F. Blackburn, 1973, "Application of Singularity Expansion Method for the Loop Antenna," *Proc. Int. Sym. On Antennas and Prop.*, pp. 470-473, IEFE Catalog No. 73CHO-764IAP, Boulder, Colorado.

10. Daniels, D. J., 1996, *Surface-Penetrating Radar*, The Institute of Electrical Engineering, London, England.

11. Nahin, P. J., 1987, *Oliver Heaviside: Sage in Solitude*, IEEE Press, New York, New York.

12 Stolarczyk, L. G., ScD., Jedlicka, R., PhD. and H. M. Tehrani, PhD., 2006, *Fox Hunter Antenna Analytical Expressions and Numerical Computations*, IEEE Antennas Propagation/URS Symposium, Albuquerque, New Mexico.

Background Patents and Applications

United States Patent Number 4,753,484, *Method for Remote Control of a Coal Shearer*, dated June 28, 1988.

United States Patent Number 5,769,503, *Method and Apparatus for a Rotating Cutting Drum or Arm Mounted with Paired Opposite Circular Polarity Antennas and Resonant Microstrip Patch Antennas and Resonant Microstrip Patch Transceiver for Measuring Coal, Trona, and Potash Layers Forward, Side, and Around a Continuous Mining Machine*, dated June 23, 1998.

United States Patent Number 5,072,172, *Method and Apparatus for Measuring the Thickness of a Layer of Geologic Material Using a Microstrip Antenna*, dated December 10, 1991.

United States Patent Number 6,497,457 B1, *Drilling, Image, and Coal-Bed Methane Production Ahead of Mining*, dated December 24, 2002.

United States Patent Number 6,522,285 B2, *Ground-Penetrating Imaging and Detection Radar*, dated February 18, 2003.

United States Patent Number 4,188,426, *Method for Controlling the Thickness of a Layer of Material in a Seam*, dated February 23, 1993.

United States Patent Number 6,633,252 B2, *Radar Plow Drillstring Steering*, dated October 14, 2003

United States Patent Number 6,778,127 B2, *Drillstring Radar*, dated August 17, 2004.

United States Patent Number 6,892,815 B2, *Coal Bed Methane Borehole Pipe Line Perforation System*, dated May 17, 2005.

United States Patent Application 654-16, *Slickline Data Transmission System*.

Provisional Application for Patent Registration Number 33,258, Docket Number MLF 654-18, *Increased Methane Production from CoalBed Deposits by Acoustic Vibration of Exhaust Wells*, dated November 19, 2004.

United States Patent Application MLF 634-19, *Earth-Penetrating Radar with Inherent Near-Field Rejection*

APPENDIX A
TECHNICAL DESCRIPTION OF LAR DEVELOPMENT

The original concept of a look-ahead radar (LAR) system was as an extension of Stolar's existing Horizon Sensor (HS) System. The concept (HS-LAR) is shown in Figure A-1.

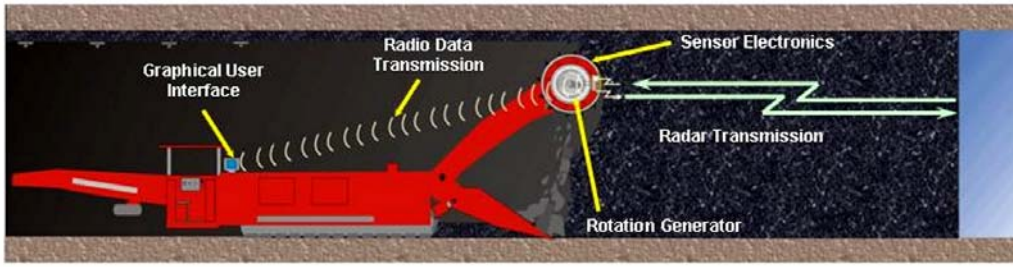

Figure A-1. Look-Ahead-Radar Detection System concept.

The antenna and electronics of the LAR system would be mounted on the surface of the coal cutting drum in the space between the spiral vanes or bit blocks, as illustrated in Figure A-2.

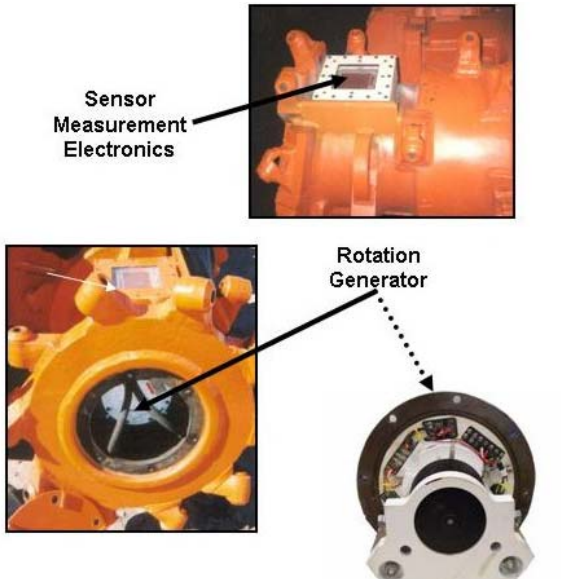

Figure A-2. Horizon Sensor mounted on mining machine cutting drum.

The sensor electronics receive electrical power from a pendulum locked-rotor generator assembly mounted in the end cavity of the cutting drum. The rotating angle must be accurately determined so that measurement occurs within ± 5 degrees of the look-up, look-forward, and

look-down antenna angles. At a drum rotation speed of 1 revolution per second, the radar measurement must be completed in 28 milliseconds. The detection sensor enclosure design was approved by MSHA as flameproof. The sensor design electronics featured high-speed microprocessors controlling the radar electronics and microwave antennas. The design successfully proved that the time-to-failure was measured in years. Thus, smart cutting drums are a reality. For the LAR, a second antenna has been added to the cutting drum. Figure A-3 is a block diagram of the cutting drum-mounted radar.

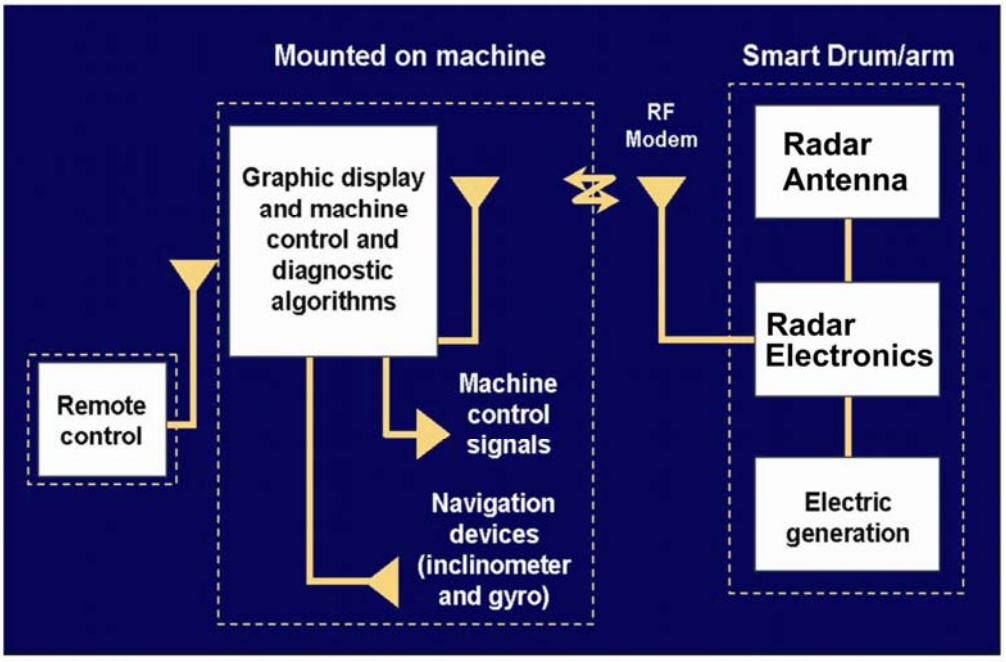

Figure A-3. Cutting drum-mounted radar block diagram.

The radar generates an electromagnetic (EM) wave that travels through the coal to the boundary layer or water- or gas-filled entry of a nearby abandoned mine. The EM wave is partially reflected at the antenna-coal interface and again at the coal-water or coal-gas interface. The distance (R) to the boundary layer or water- or gas-filled void is determined by the well-known radar equation

$$R = \frac{1}{2}\upsilon\tau \text{ meters}, \qquad \text{(A-1)}$$

Where υ is the velocity of the EM wave in the coal medium in meters per second and τ is the round trip travel time in seconds.

The travel time (τ) is determined by processing the reflected signal in the radar electronics. The distance-to-void or boundary information is transmitted by a radio-frequency (RF) modem (2.4 GHz) to the machine for display and warning on a graphical user interface (GUI). The GUI

information is transmitted simultaneously by a two-way Bluetooth[4] RF modem to the machine's remote control station. For in-mine experimental purposes, the RF modems enable IAP of the electronics and data logging during coal production.

The technical challenges will be discussed in the following paragraphs.

Electromagnetic wave reflections at the antenna-air-coal and coal-water or coal-gas interfaces are shown in Figure A-4.

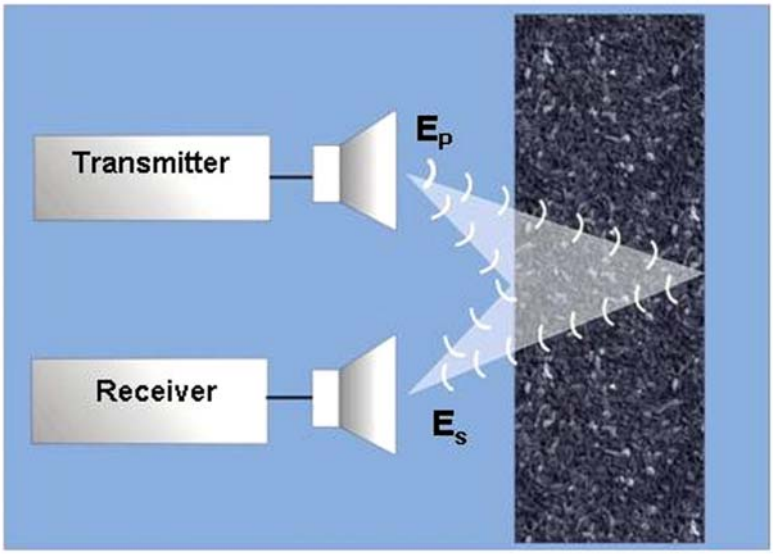

Figure A-4. Radar reflections.

The primary EM wave electric field component (E_p) travels to and is reflected by the first air-coal interface, creating a secondary electric field component (E_s) that arrives back at the receiving antenna. Part of the primary wave travels through the first interface and is reflected by the coal-water or coal-gas interface located at distance (R). The reflected wave arrives at the receiving antenna with a delay of τ seconds after the reflection from the first interface.

The EM wave reflection process is more complicated because of internal reflections occurring within the bulk coal and EM wave energy absorption (heat loss). This phenomenon is illustrated in Figure A-5.

[4] Bluetooth is a trademark of Bluetooth Sig, Inc., Bellevue, Washington.

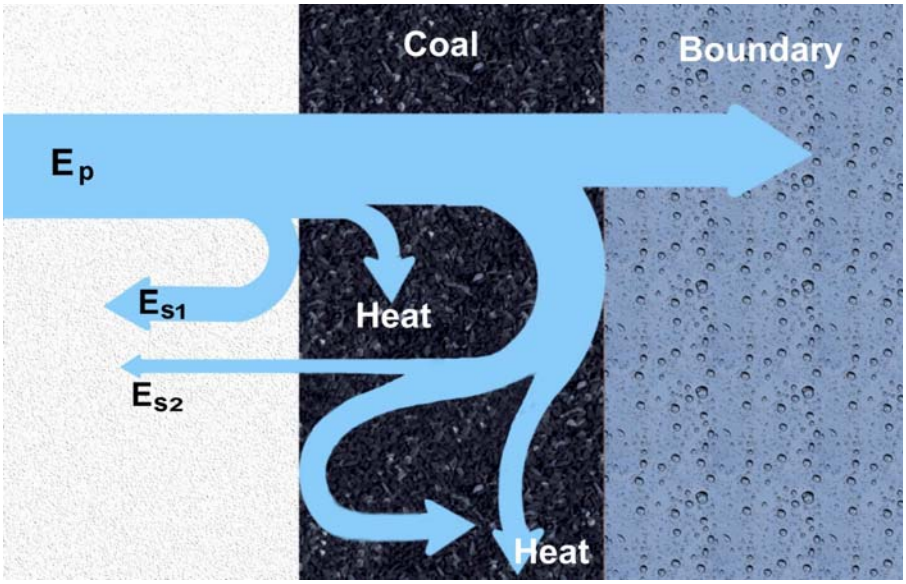

Figure A-5. EM wave energy flow in the horizon sensing and abandoned mine detection problem.

The EM wave energy (E_{S1}) reflected from the first interface is several orders of magnitude greater than the energy (E_{S2}) reflected from the second interface. The first reflection presents a number of technical challenges in the radar detection problem. First, when the first interface reflected wave energy reaches the antenna, the antenna response exhibits a radar "ring" time period before reaching steady state. The ring time will last for a few nanoseconds and interfere with detection near the first interface and weak reflections from the second interface. Although the ring time is easy to visualize in a pulse radar, a similar phenomenon occurs in a swept-frequency continuous wave (FMCW) or stepped-frequency continuous wave (SFCW) radar because of the finite frequency range in the frequency domain measurement. The transformation of frequency-domain-measured data to the time domain forms a ringing time domain response. The reflection from the first interface can saturate (overload) the sensitive amplifiers that are designed to amplify the much weaker reflected wave from the boundary layer or coal-water or coal-gas interface. In fact, antennas designed for near-field impedance measurement are needed to measure distance in thin coal layers.

A solution to the problem of measuring thin-coal-layer thickness was suggested by Chang (5, 7) and Chang and Wait (9). The Chang-Wait resonant loop sensor was not practicable for application on a metallic cutting drum, however a resonant microstrip patch antenna (RMPA) eventually was successfully developed under a grant from the U.S. National Aeronautics and Space Administration (NASA) Johnson Space Center. The sensor was evaluated for measuring ice thickness on the Orbiter low-temperature liquid fuel tanks.

The RMPA sensor was adapted for installation on the cutting drum. The HS-3 design and in-mine tests were funded to the $10-million level by Stolar Horizon, Inc.; the DOE Mine of the Future project (MOF). The participating mining companies contributed in-kind mining cost estimated to equal the development expense. This was the first wide-scale demonstration of real-

time uncut coal measurement on buckets and cutting drums of continuous mining (CM) machines, longwall shearers, and Marietta miners. The HS-3 enabled the real-time measurement of the coal layers in soft-coal conditions, but failed to meet overall expectations. The lessons learned resulted in the knowledge base to design and build a new class of radar. The mechanical design team was assisted by Sandia National Laboratories in achieving long-term sensor survivability on the cutting drum. To enable the detection of the significantly weaker reflection from the second boundary layer or coal-water or coal-gas interface, a radar technology breakthrough was needed. Specifically, the breakthrough is the combination of predistorting the transmitted EM waveform and processing the received reflected wave. The advanced radar operates in either of two distinctly different transmitted waveform modulation processes: constant and variable modulation frequency. The waveform is an amplitude-modulated, double-sideband suppressed carrier. Narrow-band and wideband antennas are used in the realization of the advanced radar. The constant modulation frequency requires wide-bandwidth antennas. Variable modulation frequency requires a tunable pair of narrow-bandwidth antennas or wideband antennas.

The advanced radar features a software-definable transceiver (SDT) and processing algorithms. Before describing the advanced SDT radar design, background development information will be summarized in the following paragraphs. The Chang and Wait sensor initially developed for boundary layer detection will be described because the design solution is applicable but did not include the rotating coal cutting drum technical problem.

The breakthrough in the radar design state of the art features the transmission of a predistorted waveform. The transmitted waveform is a double sideband suppressed carrier with the heterodyne mixed down waveform being in-phase (I) quadrature (Q) continuous waves. After mixing, bandpass filtering, and phase-coherent detection, the magnitude and phase of the reflected wave from the first (near measurement mode) and second (far measurement mode) interfaces are measured. The complex (real and imaginary) impedance of the RMPA, measured as a function of uncut coal thickness, is shown in Figure A-6.

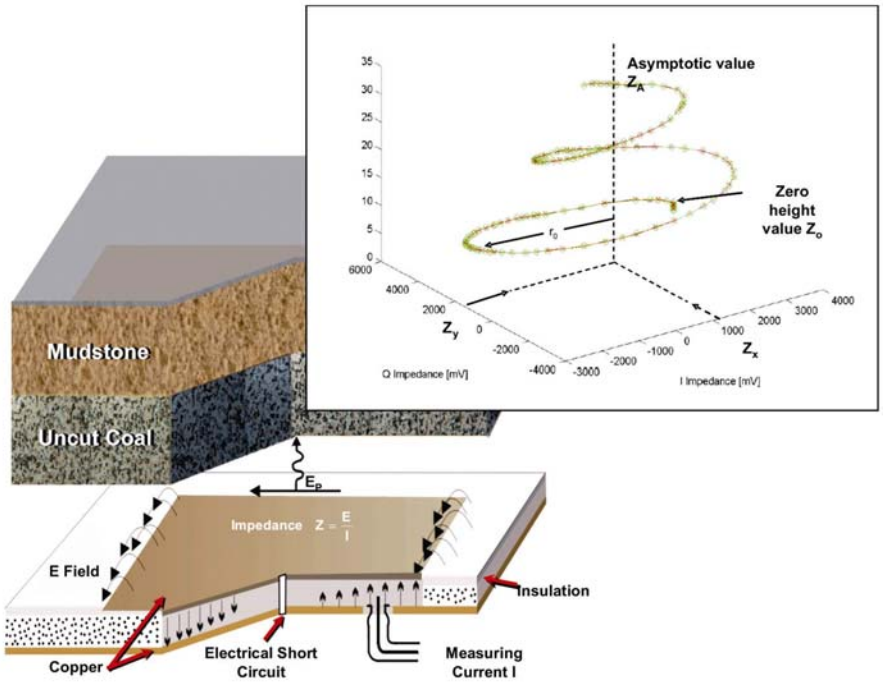

Figure A-6. Measured resonant microstrip patch antenna impedance versus uncut coal thickness in inches.

The Horizon Sensor (HS-3) radar electronics measures the impedance and compares the value to the HS-3 calibration table to determine uncut coal thickness in real time. The calibration table is established by cutting coal to a specific distance from the roof and floor sedimentary rock boundaries, then making an impedance measurement at that thickness and storing the value in the HS-3 memory. Laboratory tests were conducted using plastic barrels filled with sand-clay layers with the fine coal layer on top of the sand-clay layer. The measured results were identical to the theoretical results predicted by Chang and Wait.

In-mine demonstrations failed to achieve the theoretical and laboratory-simulation results shown in Figure A-6. Even with the best possible cooperation with underground mining machine operators, the in-mine demonstrations disrupted coal production. The disruption was an extreme problem in the development of gate roads for high-production longwalls. To minimize the disruption, the two-way Bluetooth modems were integrated into the electronics design to enable real-time remote acquisition of data. The HS-3 electronics design did not permit IAP. The in-mine demonstrations proved that IAP was an additional electronics design requirement. This enables remote reprogramming and adjusting the radar electronics while mining or drilling. When the two-way modems were incorporated into the electronics design, the drum rotation angle sensor was found to be extremely sensitive to shock, causing the random triggering of the radar measuring electronics. The HS-3 rotation angle sensor was a complex accelerometer design. The measurement trigger required the exact determination of rotation angle for looking up, forward, and down within ± 5 degrees. The mining company engineers suggested the adaptation of a Hall-effect magnetic switch detector mounted in the drum and companion magnet

mounted on the drum support beam to survive as the rotation angle detection trigger. When implemented, this suggestion solved the triggering problem.

The coal layer overlying the antenna sensor was stress-fractured coal, as shown in Figure A-7.

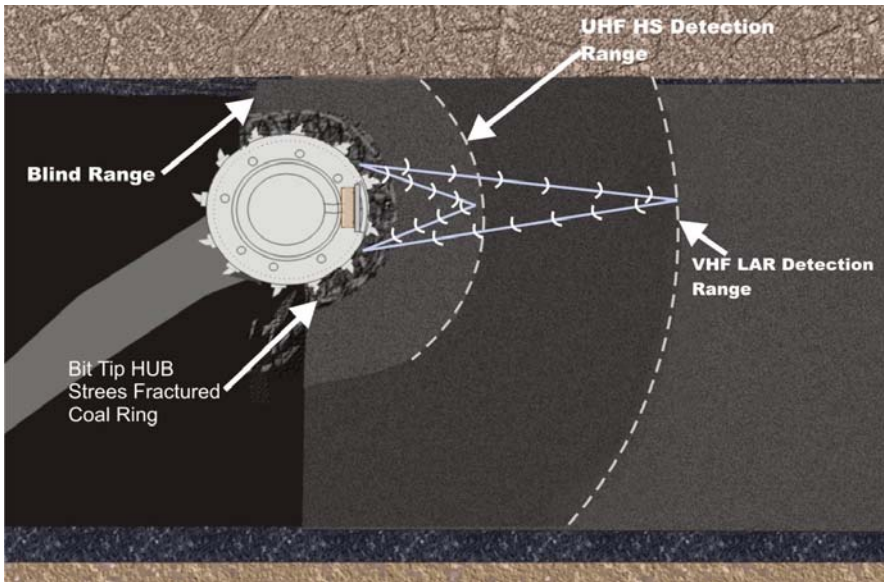

Figure A-7. HS-LAR detection problem.

The fractured coal dielectric permittivity was highly variable, causing impedance to be a random variable. Software algorithms were developed to estimate the impedance value, but were judged by the mining company to be unusable. This problem was compounded by the rotating drum sometimes cutting rock and then coal at different machine forward speeds. Additional work is needed in developing an effective algorithm for the RMPA.

Researchers have solved the problem of detecting small cross-section scatters by subtracting the time domain response from calibrated responses. This requires a stationary radar and target. Radars originally developed in World War II gate the receiver off for a time period following the transmission of the radar device. Yet another solution is to use a right-hand circular polarization for the transmit antenna (TX) and a right-hand circular polarization antenna for the receive antenna (RX). Both the TX and RX antennas have the same polarization for first interface with negative reflection coefficient (Γ). The circular polarized antenna pair will provide less than 20 dB of suppression of the first interface reflection. Still another uses a pair of antennas connected in a differencing scheme to suppress plane wave fronts reflected from the first interface. The required dynamic range of at least 80 dB, along with the hostile cutting environment prevents the adoption of these methods in coal mines.

Applying radio geophysics theory, the reflected wave occurring at each interface can be determined from the impedance, Z, of the natural medium (coal, water, or gas). The problem is similar to the acoustic wave case where acoustic impedances are applied in determining the reflection coefficient. The reflection coefficient (Γ) is mathematically given by

$$\Gamma = \frac{E_2}{E_i} = \frac{Z_2 - Z_1}{Z_2 + Z_1} \ , \qquad \text{(A-2)}$$

where E_2 = the reflected electric field at the interface,

E_1 = the incident electric field,

Z_1 = the characteristic impedance of the first medium, and

Z_2 = the impedance of the second medium.

The impedance of natural media is given by

$$Z = \frac{\sqrt{\frac{\mu}{\varepsilon}}}{\sqrt{1 - i\frac{\sigma}{\omega\varepsilon}}} \ , \qquad \text{(A-3)}$$

where σ = the electrical conductivity in Siemens per meter,

μ = $\mu_r\mu_o$ is the magnetic permeability, $\mu_o = 4\pi \times 10^{-7}$ henries/meter and μ_r is the relative permeability of the natural medium,

ε = $\varepsilon_r\varepsilon_o$ is the electrical permittivity, $\varepsilon_o = 1/36\pi \times 10^{-9}$ farads/meter, and ε_r is the relative dielectric permittivity,

and $\omega = 2\pi f$ and f is the frequency in hertz.

The ratio $\sigma/\omega\varepsilon$ is called the loss tangent. It represents the ratio of conduction to displacement current caused by EM propagation in natural media. The heat loss in the coal results in the absorption of the EM wave along the travel path expressed in terms of the Heaviside (11) attenuation rate, α.

$$\alpha = \omega\left[\frac{\mu\varepsilon}{2}\left(\left[1+\left(\frac{\sigma}{\varepsilon\omega}\right)^2\right]^{\frac{1}{2}} - 1\right)\right]^{\frac{1}{2}} \text{ nepers per meter,} \qquad \text{(A-4)}$$

and the phase constant

$$\beta = \omega\left[\frac{\mu\varepsilon}{2}\left(\left[1+\left(\frac{\sigma}{\varepsilon\omega}\right)^2\right]^{\frac{1}{2}} + 1\right)\right]^{\frac{1}{2}} \text{ radians per meter.} \qquad \text{(A-5)}$$

Equations A-4 and A-5 simplify when the loss tangent $\sigma/\varepsilon\omega$ is much, much greater than unity as

$$\alpha = \beta = \sqrt{\frac{\omega\mu\sigma}{2}} \ ; \frac{\sigma}{\omega\varepsilon} >> 1 \ . \qquad \text{(A-6)}$$

The impedance simplifies to

$$Z = \sqrt{\frac{j\omega\mu}{\sigma}} = \sqrt{\frac{\omega\mu}{\sigma}} \quad \angle 45^\circ , \tag{A-7}$$

where j is equal to $\sqrt{-1}$ and $\alpha \approx 55$ dB/λ. When the loss tangent is much, much less than unity,

$$\alpha = \frac{\sigma}{2}\sqrt{\frac{\mu}{\varepsilon}} \text{ and } \beta = \omega\sqrt{\mu\varepsilon}\,; \ \frac{\sigma}{\omega\varepsilon} << 1 , \tag{A-8}$$

the impedance is given by

$$Z = \frac{377 \ ohms}{\sqrt{\varepsilon_r}} \ . \tag{A-9}$$

The wavelength in any medium is given by

$$\lambda = \frac{2\pi}{\beta} \text{ meters.} \tag{A-10}$$

Tables A-1 and A-2 list the EM wave propagation parameters for a wide range of natural media. Table A-1 assumes a relative dielectric permittivity of 4; Table A-2 assumes values often given in petrophysics articles. Natural media exhibit a complex dielectric permittivity given by $\varepsilon = \varepsilon' - j\varepsilon''$, where ε' is the real part and ε'' is the imaginary part. From Maxwell's first equation,

$$\nabla \mathrm{XH} = \varepsilon \frac{d\mathrm{E}}{dt} , \tag{A-11}$$

where H is the magnetic field component, and E is the electric field component, we have

$$\nabla \mathrm{XH} = \left[\omega\varepsilon'' + j\omega\varepsilon'\right]\mathrm{E} . \tag{A-12}$$

The electrical conductivity is mathematically given by

$$\sigma = \omega\varepsilon'' \tag{A-13}$$

Laboratory and in situ measurements of conductivity exhibit first power of frequency dependence.

Table A-1. Electromagnetic Wave Parameter Preparation.

Modulation Frequency ($(\omega_m = \omega_1 + \omega_2)/2$) (MHz)	**Loss Tangent ($\sigma/\varepsilon\omega$)**	**Attenuation Rate (α) (dB/ft)**	**Phase Constant (β) (Rad/m)**	**Wavelength ($=2*\pi/\beta$) (m)**	**Wavelength (λ) (ft)**
1	2.25	0.09	0.06	113.97	373.93
3	0.75	0.12	0.13	47.11	154.58
10	0.22	0.12	0.42	14.90	48.88
30	0.07	0.12	1.26	4.99	16.38
60	0.04	0.12	2.52	2.50	8.20
100	0.02	0.12	4.19	1.50	4.92
300	0.01	0.12	12.58	0.50	1.64
$\sigma = 0.005$ S/m $\varepsilon_r = 4$					
1	22.47	0.36	0.14	43.74	143.50
3	7.49	0.60	0.26	24.16	79.26
10	2.25	0.95	0.55	11.40	37.39
30	0.75	1.18	1.33	4.71	15.46
60	0.37	1.23	2.56	2.46	8.06
100	0.22	1.24	4.22	1.49	4.89
300	0.07	1.25	12.58	0.50	1.64
$\sigma = 0.05$ S/m $\varepsilon_r = 4$					
1	224.69	1.17	0.45	14.11	46.29
3	74.90	2.02	0.77	8.11	26.61
10	22.47	3.64	1.44	4.37	14.35
30	7.49	6.03	2.60	2.42	7.93
60	3.74	7.98	3.93	1.60	5.25
100	2.25	9.48	5.51	1.14	3.74
300	0.75	11.76	13.34	0.47	1.55

The velocity (υ) is given by

$$\upsilon = \frac{\omega}{\beta} \text{ meters per second.} \qquad \text{(A-14)}$$

The wavelength also is given by

$$\lambda = \frac{\upsilon}{f} \ . \qquad \text{(A-15)}$$

The round-trip phase shift in the reflected wave is given by

$$\varphi = 2\,R\beta \text{ radians} \qquad \text{(A-16)}$$

from Equations A-1 and A-10,

$$\varphi = \omega\tau \text{ radians,} \qquad \text{(A-17)}$$

where $\omega = 2\pi f$ is the modulation or suppressed carrier frequency.

Nominal values for the electrical parameters for coal, shale, lake water, limestone, and air are given in Table A-2.

Table A-2. Electrical Parameters for Coal, Shale, Lake Water, and Air. (7)

Surface	**Electrical Parameter**		**Frequency**			
			(1 MHz)		**(100 MHz)**	
	σ (S/m)	**ε_r**	$\frac{\sigma}{\omega\varepsilon}$	$\lvert Z\rvert$	$\frac{\sigma}{\omega\varepsilon}$	$\lvert Z\rvert$
Dry coal	0.0005	4	2.247	120.1	0.022	188.3
Saturated shale	0.05	7	128.4	12.6	1.284	111.6
Lake water	0.02	81	4.44	19.6	0.044	41.8
Limestone	0.001	9	2.00	84.0	0.020	125.6
Air	0	1	0	376.7	0	376.7

Using the values provided in Table A-1 corresponding to a conductivity of 0.0005 S/m and a permittivity of 4 were used to calculate the velocity in coal at 100 MHz to be 1.49 x 10^8 m/sec or 0.49 ft/nanosec. The attenuation rate is 2.35 dB/m (Pittsburgh seam) and 4.1 dB/m (Illinois seam).

The reflection coefficients for coal-water, coal-air, air-coal, and coal-rock interfaces are given in Table A-3 at 1 MHz and in Table A-4 at 100 MHz. The values in Table A-2 were used to obtain these reflection coefficients.

Table A-3. The Reflection Coefficient (Γ) at 1 MHz.

Coal-Water	**Coal-Air**	**Coal-Rock**
0.71 (-3 dB)	0.51 (-5.7 dB)	0.81 (-1.8 dB)

Table A-4. The Reflection Coefficient (Γ) at 100 MHz.

Coal-Water	Coal-Air	Coal-Rock
0.63 (-4 dB)	0.34 (-9.4 dB)	0.25 (-12 dB)

The EM wave energy velocity (υ) is determined from the first interface reflection response. While the petrophysics and geology provide this response independent of the instrumentation, the LAR electronics are vastly different for the original Horizon Sensor system.

The breakthrough in the state of the art was achieved by developing a radar technology that can operate in both near and far measurement modes. The near mode measures the much larger reflected waveform, the first interface. This measurement mode also determines the predistortion requirement at each waveform frequency component (the two sidebands). The first interface reflection coefficient (Γ_1) follows by substituting Equation A-3 into Equation A-2 as

$$\Gamma_1 = \frac{\sqrt{\varepsilon_1} - \sqrt{\varepsilon_2}}{\sqrt{\varepsilon_1} + \sqrt{\varepsilon_2}} \, . \tag{A-18}$$

Solving for the relative dielectric permittivity (ε_2) of coal,

$$\varepsilon_2 = \varepsilon_1 \left(\frac{1-\Gamma_1}{1+\Gamma_1} \right)^2 , \tag{A-19}$$

where ε_1 is the relative dielectric permittivity of the protective layer covering the antenna.

Assuming the EM wave reflected from the air-coal second interface at 20 ft (12.9 m) is significantly smaller in amplitude than the EM wave reflected from the first interface. The reflected signal from the coal, hydrocarbon reservoir boundary rock, or abandoned mine undergoes various losses in its path from the SDT transmitter to the receiver. The total path loss for a particular distance is given by

$$L_T = L_{ef} + L_{MM} + L_s + L_{\Gamma 1} + L_{\Gamma 2} + L_{R1} + L\alpha \, , \tag{A-20}$$

where

L_{ef} = antenna efficiency loss = 6 dB,

L_{MM} = antenna mismatch loss = 1 dB,

L_s = antenna spreading loss[5] = 16 dB,

$L_{\Gamma 1}$ = transmission loss through the first interface = 3.6 dB,

[5] Spreading loss from the planar second interface will be less by approximately 7 dB.

$L_{\Gamma 2}$ = reflection loss at the second interface = 9.3 dB,

L_{R1} = reflection loss at the first interface = 3.6 dB, and

$L\alpha$ = attenuation loss in natural media:

for the Pittsburgh seam:

12.1 m x 2.35 dB/m = 28.4 dB, and

for the Illinois seam,

12.1 m x 4.1 dB/m = 49.6 dB.

The total loss for the Pittsburgh seam is 67.9 dB.

The total loss for the Illinois seam is 89.1 dB.

At 1 MHz, limestone with a saturated shale boundary has an attenuation rate in limestone of 0.97 dB/m and a wavelength of 57.1 m. The reflection coefficient is 0.73 (-2.7 dB).

Consider the basic physical system, shown in Figure A-8.

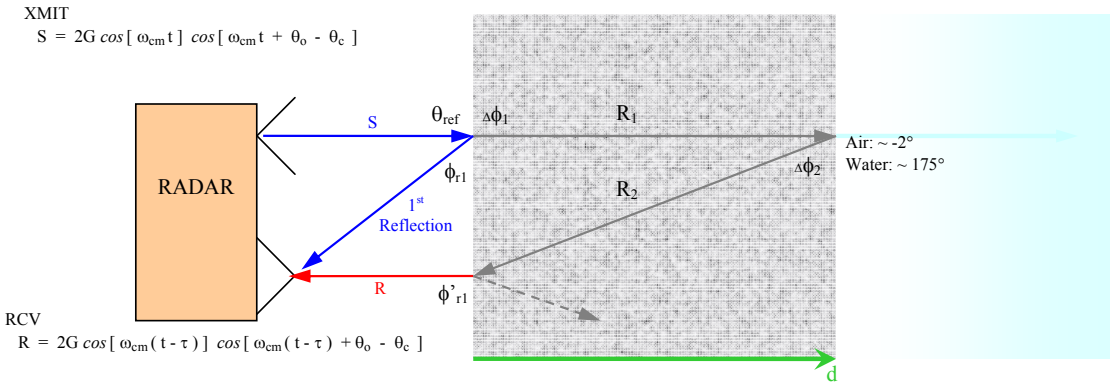

Figure A-8. Model of basic physical system.

A transmitted signal (S) impinges on the coal interface at some reference angle (θ_{ref}), which is, for convenience, assumed to be 0°. A significant portion of this signal is reflected back to the receive electronics at some angle (ϕ_{r1}).

The signal undergoes a phase shift—$\Delta\phi_1$—as it passes through the interface. This wave then passes through the coal and is attenuated to some degree and undergoes additional phase shift—some amount R—that is related to the material properties incorporated in the parameter (β) over some distance (d) to the void interface.

$$\varphi_{r1} = \text{first reflection} = 179.5° \qquad \text{(A-21)}$$

$$\Delta\varphi_1 = \text{through interface} = 21.4° \qquad \text{(A-22)}$$

Some portion of this wave is reflected off the void interface, the degree of which is determined by the properties of the void. If the void is air filled, a phase shift —$\Delta\phi_2$—of something near 2° occurs; if the void is water filled, the phase shift is about 175°—close to a 180° difference. The signal energy transmitted into the void is lost forever.

The reflected portion of the signal is again attenuated through the coal on the return and has the same associated phase shift of R. This wave returns to the first coal interface where a certain portion is transmitted back through the interface to the receiver; a certain portion is reflected back into the coal to repeat the process. (This signal is properly represented as an infinite series of reflection-transmissions, but we only discuss the first sequence for brevity).

The portion of the wave passing back through the coal-air interface undergoes another phase shift (ϕ'_{r1}), which then is ideally detected by the receive electronics.

Properly speaking, the parameter τ is a function of time. However, as may be seen in the expression from which τ is measured, a frequency component (ω_o) is associated with it. It may be assumed that each phase term consists of ω_o and an associated time shift—this combination of ($\omega_o\tau$) will be stated as some angle ϕ. Note that ω_o is constant for the entire system and each term.

An expression for τ was derived as

$$\tau = \frac{\tan^{-1}\left(\frac{Q}{I}\right) - \theta_c}{\left(\omega_o + \frac{\omega_2 - \omega_1}{2}\right)} \quad , \qquad \text{(A-23)}$$

which is derived from the radar signal components I and Q expressed as

$$I = \frac{1}{2}\cdot\cos\left(\omega_m\tau + \theta_m\right)\cdot\cos\left(\omega\tau + \theta_{cm}\right) \qquad \text{(A-24)}$$

and

$$Q = \frac{1}{2}\cos\left(\omega_m\tau + \theta_m\right)\cdot\sin\left(\omega_{cm}\tau + \theta_{cm}\right) \ , \qquad \text{(A-25)}$$

where ω_m is the modulation frequency (angular),
θ_{cm} is the phase of the modulation carrier frequency,
ω_{cm} is the modulation carrier frequency (angular), and
θ_c is the phase of the carrier frequency.

The symbol "ϕ" is used to differentiate between the phase shifts designated "θ," which are associated with the inter-workings of the radar electronics and those associated with the physical system to be measured.

Furthermore, it is noted that the phase constant "β" (see Equation A-4) is a material-dependent phase propagation constant where β has units of radians per meter. Multiplying this by distance traveled results in the amount of phase shift expected.

An expression for τ is stated as:

$$\tau = \phi_{r1} + \Delta\phi_1 + \beta R_1 + \Delta\phi_2 + \beta R_2 + \Delta\phi'_{r1} \Rightarrow \phi_{r1} + \Delta\phi_1 + \Delta\phi_2 \text{ (void)} + \Delta\phi'_{r1} \text{ (passing through first interface)} + 2R\beta \quad \text{(A-26)}$$

out of which R is the parameter to be determined. (Note that it is assumed that $R_1 = R_2$.)

Using the following parameters: $\varepsilon_{r,coal} = 4$, $\sigma_{coal} = 0.0005$, f = 200 MHz, and an air-filled void,

$$\tau = 179.5°(\text{if suppressed} = 0) + 21.4° + 2\,(9.3°) + 0 + (-107.3°) = 112° \quad \text{(A-27)}$$

The radar frequency transposition scheme occurs simultaneously so that both the in-phase (I) and quadrature (Q) signals are received after the 455-KHz intermediate-frequency filter.

The magnitude of the phase-coherent detector signals becomes

$$M = \left| I^2 + Q^2 \right|^{1/2} = \left| \cos\left(\theta_m + \omega_m \tau\right) \right| \quad \text{(A-28)}$$

and phase

$$\theta_c + \omega_{cm}\tau = \tan^{-1}\frac{\theta}{1} \,. \quad \text{(A-29)}$$

For the FMCW or SFCW radar realizations, the phase shift ($\omega_m\tau$) in the modulation waveform can be determined by measuring the magnitude of the intermediate amplifier signal as the suppressed carrier frequency is swept or stepped through the radar operations frequency range. Because cos ($\omega_m\tau$) is a constant at each frequency change involved (Δf), the $\omega_m\tau$ is found as the solution of simultaneous equations.

The radar radiates a sequence of N incrementally spaced linear frequency (ω_c) steps through the 120- to 220-MHz frequency band. The frequency spectrum may be represented by a sequence of phasors:

$$E_{ro} = \sum_{n=0}^{k} M_o e^{i\theta_n} \,. \quad \text{(A-30)}$$

A complex inverse fast Fourier transform or equivalent algorithm is then used to produce a time domain version of the reflected signal illustrated in Figure A-9. The suppression of the first interface reflected wave occurs when θ_m is set by the microprocessor code to a value of π/2 in the

FPGA digital heterodyne frequency generation. The magnitude (M) function is presented mathematically by Equation A-28, and graphically by Figure A-9.

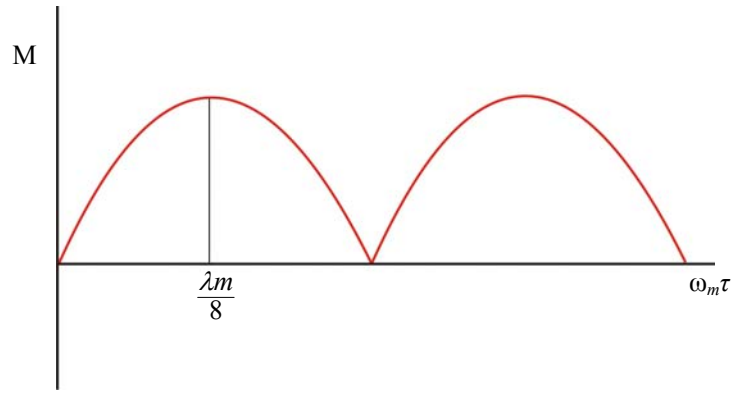

Figure A-9. Suppressing the magnitude of the reflected wave from the first interface.

The modulation phase angle, φ_m, is the product of modulation frequency ω_m and the round trip travel time, τ. The suppression in decibels as a function of phase angle, φ_m, is given in Table 2-5.

Table A-5. Suppression in Decibels.

φ_m (degrees)	Decibels
0.001	60
0.05	55
0.5	41
1.0	35
2.5	27
3.0	22
10.0	15
20.0	9
30.0	6
40.0	3.8

Because τ is the round-trip time of the reflection, the reflection from the first interface occurs at $\tau = 0$ second. The magnitude is suppressed to more than 40 dB. For a modulation frequency of 1 MHz, the wavelength λ_m in the natural coal medium is

$$\lambda_M = 374 \text{ ft } (114 \text{ m}) . \qquad \text{(A-31)}$$

The magnitude of the reflection from the second interface reaches maximum value at $\lambda_M/8$ distance of 14.2 meters. At 12.9 meters, the magnitude function (sin 40°) is only 3.8 dB less than the maximum magnitude condition at $\lambda_m/8$. If the modulation frequency is set to 60 MHz, the λ_m = 8.2 m and the reflection reaches maximum value at 1 meter.

The carrier phase (θ_c) in Table A-5 can be set by the microprocessor controller to adjust the FPGA. The microprocessor can set θ_c so that $\theta_c + \omega_{cm}\tau = 0$. Because ω_{cm} is at the operating frequency of the radar, the wave length in coal

$$0.62 \text{ m} \leq \lambda_{cm} \leq 1.07 \text{ m}. \qquad \text{(A-32)}$$

The I and Q values exhibit an oscillation that interferes with the transformation to the time domain. Because θ_c can be set by the microprocessor, $\theta_c = \omega_{cm}\tau$ can be set to 0, eliminating the source of error in the time domain.

The suppressed carrier double-sideband transmit signal may have a variable frequency separation. This is achieved with a variable modulation frequency. The peak of the magnitude function ($\lambda/8$) can be moved to the boundary, creating a maximum value in determining range.

APPENDIX B
MINE NO. 84 FIELD TESTS, SEPTEMBER 2006

B1.0 MINE 84 TEST PROCEDURES

B1.1 Static Test Site

Testing at the static test site included two principle methodologies: transmission tests and reflection tests. Transmission testing involved placing the TX and RX units on opposite sides of the pillar to measure propagation characteristics in the coal. Reflection tests involved using the TX and RX units side by side to measure the distance to a reflecting boundary within the coal seam. Additional variations occurred in the test plan when the void-stimulant chamber was first tested empty (air-reflector), and then filled with just over 4 ft of water. The chamber provided a large, seam-height reflector for radar waves that approximates an abandoned mine entry. With the chamber filled, the boundary provided an antenna-height air-coal reflector at the same distance. A diagram of the static test site is shown in Figure B-1.

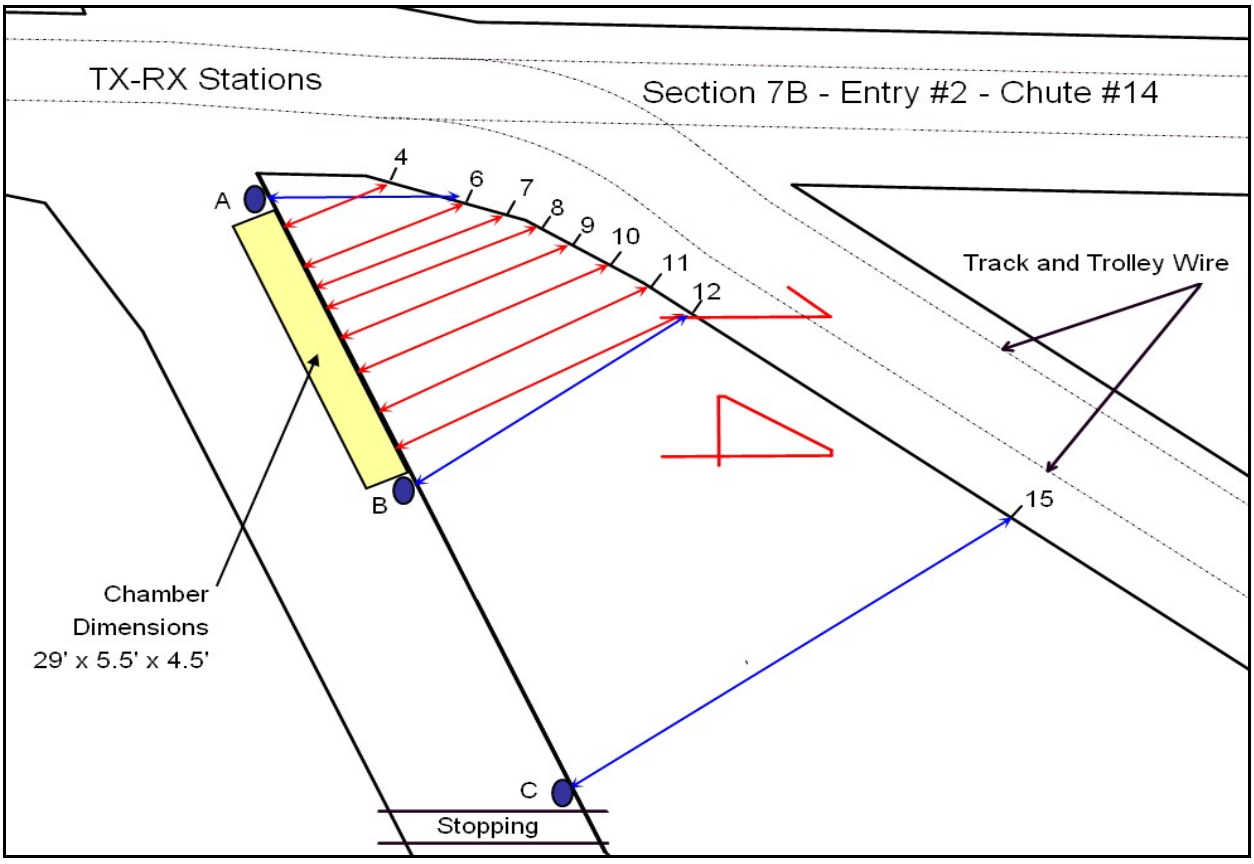

Figure B-1. LAR static test site: No. 84 Mine Cross-Cut #14/13A.

B1.2 Transmission Test Procedures

The TX unit was placed within 1 ft of the XC-13A rib and controlled by a signal generator. The RX unit was placed within 1 ft of the empty water chamber and controlled by a spectrum analyzer. Radar signals are propagated through the coal pillar at three discrete measurement stations. Each station pair represents increasing coal pillar width (15 ft, 30 ft, and 47 ft). This procedure is diagrammed in Figure B-2.

Stolar engineers defined the location of the measurement stations and test equipment using way-points provided by mine surveyors.

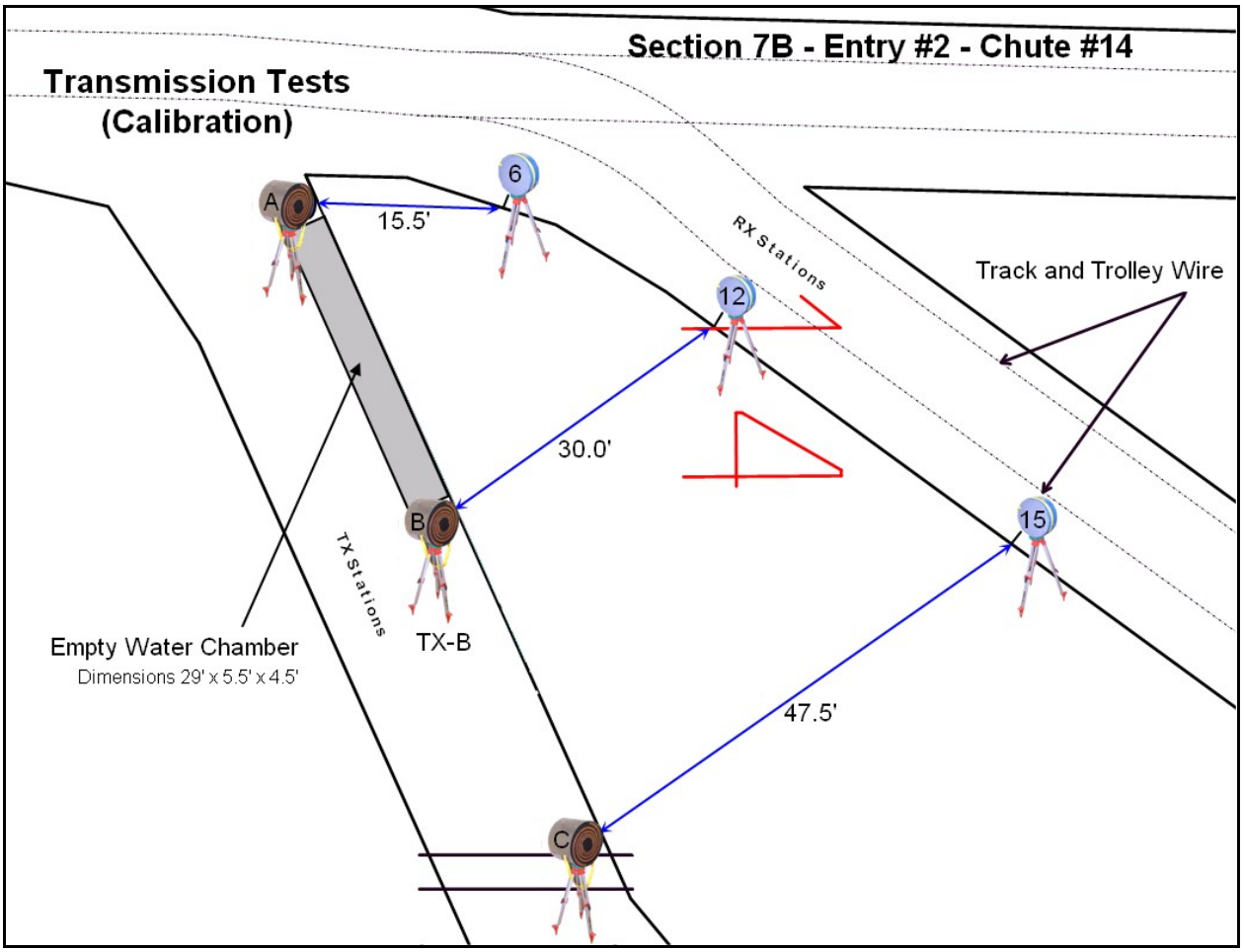

Figure B-2. LAR transmission test diagram, Static Test Site #14/13A.

B1.3 Reflection Test Procedures

Following the transmission tests, the TX and RX units were connected in a transceiver array with an optimal antenna orientation determined through transmission testing. The antennas were driven by the LAR electronics module and controlled by the laptop PC (via wireless link). The LAR transceiver was placed within 1 ft of the XC-14 rib. Radar signals were propagated

through the coal pillar at four discrete measurement stations while the PC processed and recorded reflection data. Each station pair represents increasing coal pillar width (Station #6 = 16 ft … Station #12 = 30 ft). This procedure was done using test equipment and the SDT-LAR electronics. Data were collected using the process with the chamber empty, and filled (4-ft depth). The test setup for both the empty and filled condition is diagrammed in Figures B-3 and B-4, respectively. Data was also collected while the chamber was being filled. Its depth was correlated to LAR data using a time stamp in the digital logs, as well as a water-level log kept by onsite personnel (Table B-1).

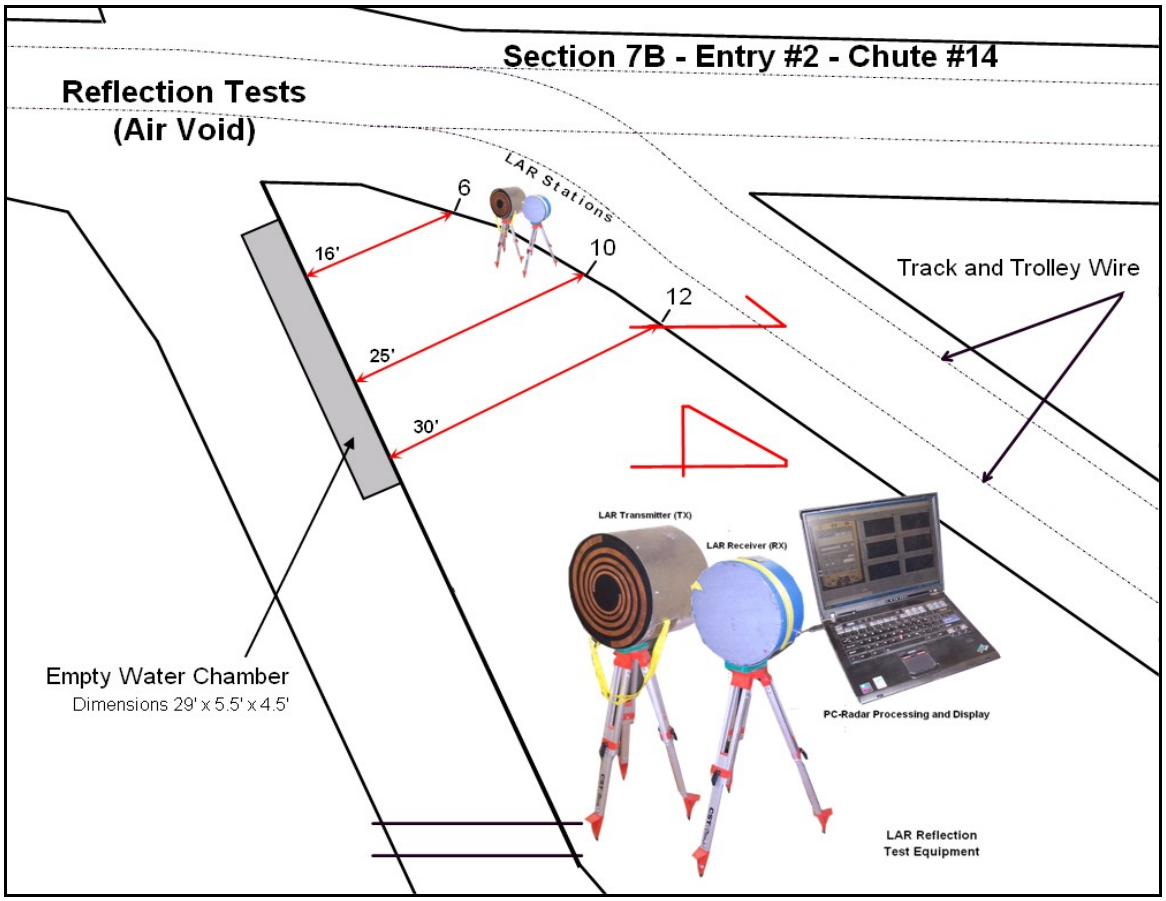

Figure B-3. Look-Ahead Radar *Air-Reflection* test diagram, Static Test Site XC-14.

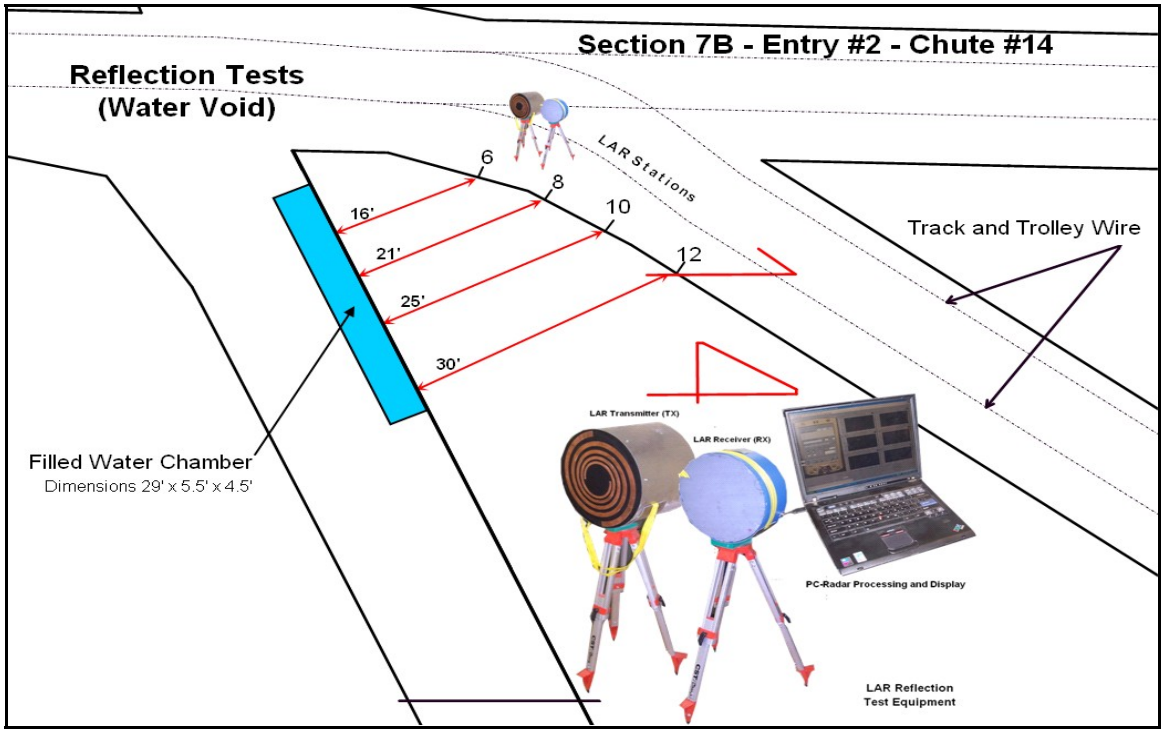

Figure B-4. Look-Ahead Radar *Water-Reflection* test diagram, Static Test Site XC-14.

Table B-1. Water Chamber Depth Log.

Time	Water Depth (ft) within Lined Chamber	Height of Water (ft) between Liner and Rib	
7:15	2.2	0	
7:30	2.4	0	← Likely position of BASE of Antennas for most data sets
7:45	2.6	0	
8:00	2.8	0	
8:15	2.9	0	
8:30	3.1	0	
8:45	3.2	0	
9:00	3.4	0	
9:15	3.6	0	
9:30	3.8	0	
9:45	3.9	0	
10:00	4.1	0	← Likely position of TOP of Antennas for most data sets
10:15	4.3	0	
10:30	4.4	1	
10:45	4.4	2	
11:00	4.4	3	

B1.2 COMMERCIAL TEST EQUIPMENT

During a small portion of the LAR testing, the transceiver was modified into stand-alone TX and RX submodules for the purpose of collecting transmission data. The antennas used for these transmission tests were the same units described earlier, however, the SDT and PC were not used, but instead the system was controlled by commercial test equipment. A Marconi-brand signal generator (SG) was used as a TX signal source while a HP-brand spectrum analyzer (SA) was used to receive and record signals. The transmission testing equipment is shown in Figure B-5.

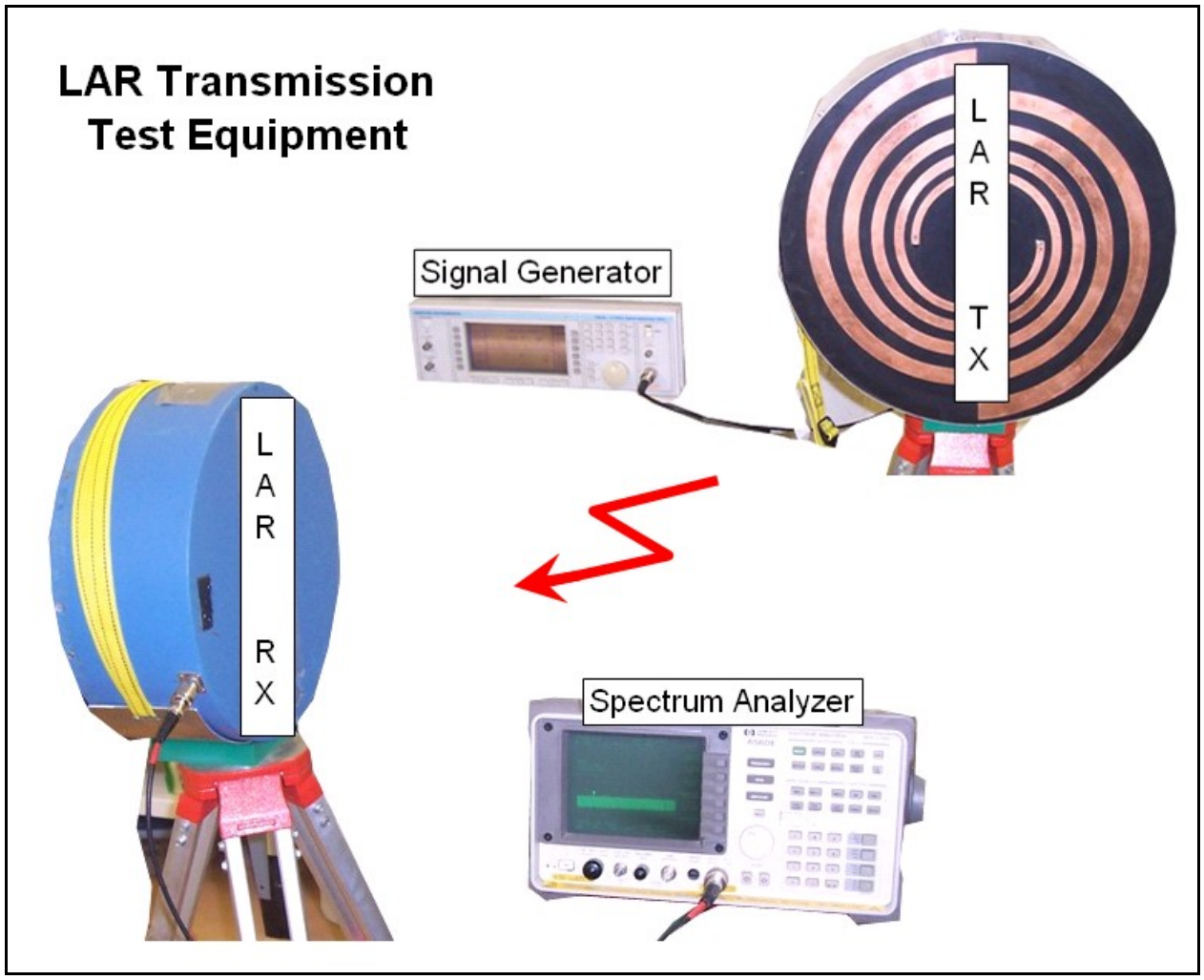

Figure B-5. Look-Ahead Radar test equipment (stand-alone modes with test interfaces).

B1.3 POWER SOURCES AND MISCELLANEOUS EQUIPMENT

The LAR system ran entirely from small self-contained VDC battery packs. These packs provided 12 to 15 VDC at currents levels below 2 A. All battery packs were sealed and fuse

protected. The commercial test equipment used 115 VAC at current loads below 5 A. This power was derived from power inverters connected to higher capacity DC battery packs brought to the static test site specifically for this purpose. The inverters and larger VDC batteries are also sealed and fuse protected. Additional equipment needed for the tests included signal cables, laptop computers (internal batteries), and tool kits.

B2.0 TEST RESULTS

B2.1 TRANSMISSION TEST RESULTS

The LAR unit collects information that ultimately depends on the propagation velocity of the electromagnetic wave through the coal medium. This velocity is calculated from

$$\upsilon = \frac{\omega}{\beta} \text{ meters per second,}$$

where

$$\beta = \omega \sqrt{\frac{\mu \varepsilon}{2} \left(\sqrt{1 + \left(\frac{\sigma}{\varepsilon \omega} \right)^2} + 1 \right)} \text{ radians per meter.}$$

In most situations, the magnetic permeability μ can be assumed to be equal to 1, leaving the dielectric permittivity ε and conductivity σ as variable material properties. Typical values for ε may range between 3 and 20 depending on a variety of factors, primarily water content, while the conductivity value may vary over many orders of magnitude—approximately 0.1 to 0.0005 S/m.

The transmission test data were collected to further match theory and practice as well as calibrate the radar unit.

These measurements were made with calibrated commercial test equipment. A suitable signal source drove the transmission antenna that directed the wave through a coal seam with known dimensions. The receiving antenna was monitored with a spectrum analyzer and the results were analyzed. Hindsight strongly suggests that the capability to also measure phase response would have been desirable.

Based on the collected data, it appears that valid numbers for analysis suggest an antenna frequency response range of 170 to 280 MHz (desired: 100 to 300 MHz). The attenuation rate is approximated as 2.4 dB/m at 190 MHz (which represents a loss of about 29 dB for a target 6 m [20 ft] distant). With an antenna transmission system loss of about 41 dB, the system needs sufficient transmission power to provide 70 dB above the noise floor. (In this test, the noise floor was at about -87 dB).

As a result of this information, it is felt that the dynamic range of the radar electronics needs to be improved. The antennas need to be better matched to the necessary frequency range and an improvement in antenna-radar impedance matching should provide increased sensitivity.

B2.2 REFLECTION TESTING RESULTS

The primary purpose of this testing was to validate the LAR system performance. Transmit and receive antennas were placed side by side and the LAR activated. As a verification, commercial test equipment also was used to collect data. A network analyzer was configured to make measurements using identical antenna placement and system as with the LAR measurements

Data were collected at four stations along the coal face. Station 6 represents the nearest target but introduces scattering effects caused by the nearness to the apex of the two entries. Station 12 represents the farthest distance and was purposely selected to miss the water bunker to provide a basis for comparison.

The layout at the test site was such that we were able to collect data in a region where no voids or artifacts were known. Because of the attenuation factor, it was estimated that a distance of more than 60 ft was sufficient to represent this no-void condition.

The results of the parallel measurements with the test equipment provide a clue. Four data sets were collected: both amplitude and phase of the S11 (input) and S21 (transmission) parameters. Keeping in mind that the information desired is contained in the phase shift, the following figures (B-6 through B-8) will illustrate the dilemma and the clue for further advancement of this project.

Figure B-6 shows the results of the amplitude measurements over a frequency range of 100 to 500 MHz. The antenna response at about 170 MHz is very prominent; the cutoff at 280 MHz or so is less discernible. The sequence of data at the top of the Figure B-6 shows the S11 input characteristics. These should be very close to identical; the input loading should not be dependent on the system transmission characteristics.

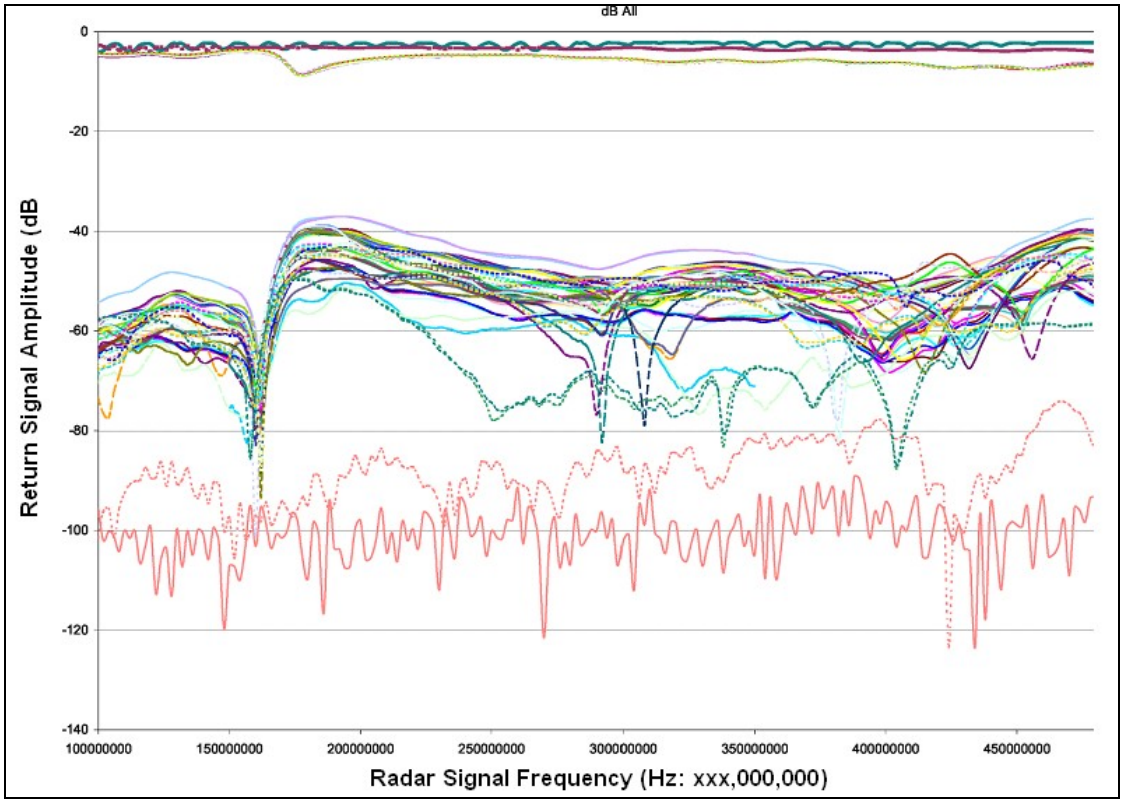

Figure B-6. LAR amplitude measurements over a frequency range of 100 to 500 MHz.

The middle grouping represents the S21 transmission characteristics; these are shown in Figure B-7. Although the geophysical information desired is contained within the phase, the variations within this grouping represent changes in attenuation parameters for each measurement location.

The lowest grouping is of the noise level. This information is primarily of importance to system development and does not directly relate to the LAR information.

The phase information collected with the network analyzer demonstrates the feasibility of continued development and suggests that perhaps the sensitivity of the LAR unit is too low and/or the processing algorithm needs modification.

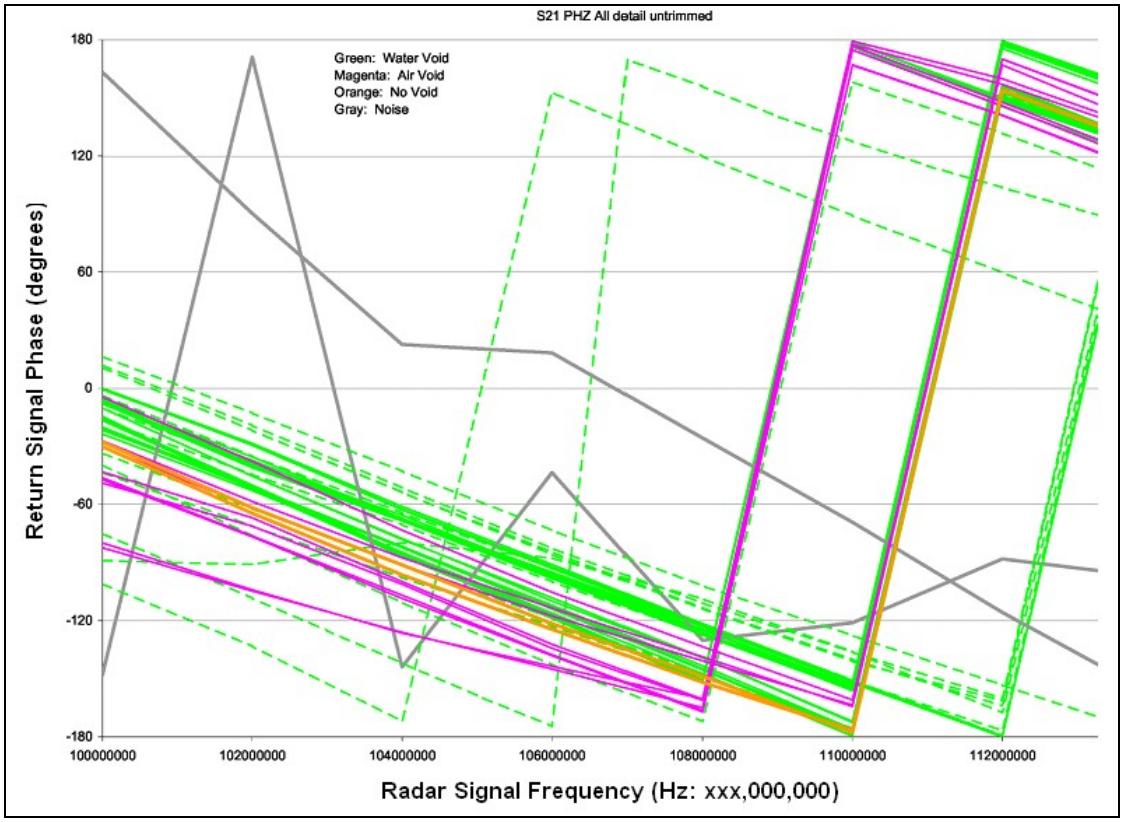

Figure B-7. The S21 transmission characteristics from Mine No. 84 LAR data.

The information in Figure B-7 is more complex to interpret because of the variations in test parameters at each station. As expected and desired, the S11 phase information may be considered identical for all intents and purposes and is therefore not shown. However, some generalizations of the presented S21 phase data may be noted.

As noted on Figure B-7, the data are color-coded as to air-filled and water-filled voids, no void, and noise. Figure B-7 presents all data collected; there are a couple of anomalous data sets caused by test parameter variations. Figure B-8 is identical to Figure B-7 with the anomalous data sets removed.

In Figure B-8, the desired grouping is very noticeable. The data were collected in "Phase Wrapping" mode where the phase is presented as fitting between ±180°. Hindsight once again appears; it would have been desirable to collect these data as a continuous function.

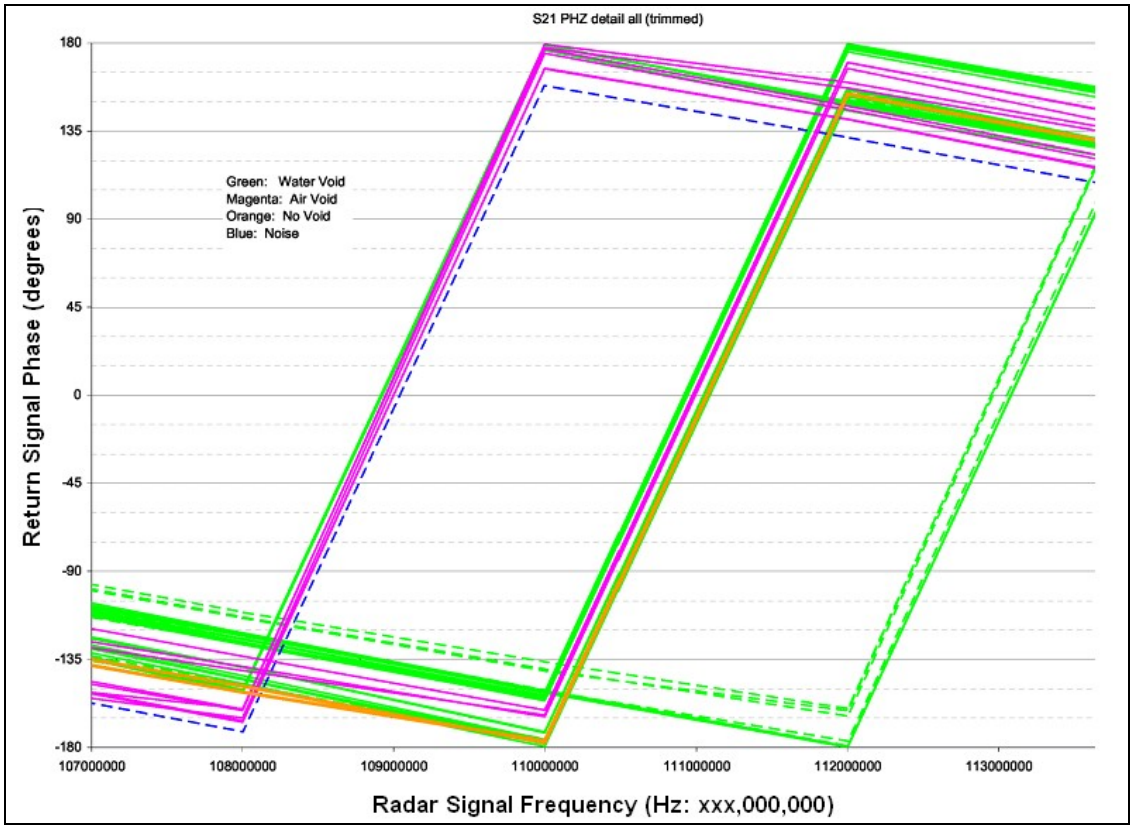

Figure B-8. Mine 84 LAR data collected in "Phase-Wrapping" mode.

It is noted that the no-void condition roughly separates the air- and water-filled void data. The basic geophysical theory predicts a significant phase difference between the reflections from an air-void and water-void[6] with the no-void condition having a phase shift nominally representing only the system phase shifts. It is interesting to note that the phase shifts that appear to be significant here can be defined from the initial data points.

The information presented here indicates two things:

- The LAR test system did not work as expected.
- The information collected indicates that the desired information is present and may be extracted if certain changes are successfully implemented. These changes are discussed elsewhere in this document.

[6] Ignoring electronic system phase shifts, the primary geophysical phase shifts result not only from the travel distance through the medium—the basic parameter of a radar system—but from interactions at points of material property changes and scattering from the roof/floor interface and fracturing within the coal seam as well. The difficulty comes from separating the effects of these different error sources of phase shift from those desired.